

Hadron physics with functional methods

Gernot Eichmann^a

^aUniversity of Graz, NAWI Graz, Institute of Physics, Universitätsplatz 5, 8010 Graz, Austria

© 20xx Elsevier Ltd. All rights reserved.

Chapter Article tagline: update of previous edition, reprint.

Contents

Nomenclature	1
Objectives	2
1 Introduction	2
2 Quarks	3
2.1 Dynamical mass generation	3
2.2 An illustrative model	4
2.3 About renormalization	5
3 Mesons	6
3.1 Bethe-Salpeter equation	6
3.2 Chiral properties of the pion	7
3.3 Bethe-Salpeter kernel	8
3.4 An illustrative model (continued)	9
4 Baryons	10
4.1 Baryons made of three valence quarks	10
4.2 Diquarks	11
5 Four-quark states	12
5.1 Dynamical generation of resonances	12
5.2 Heavy exotics	13
6 Hadron structure	15
7 Conclusions and outlook	16
Acknowledgments	16
References	16

Abstract

We give a pedagogical introduction to hadron spectroscopy and structure studies using functional methods. We explain the basic features of Dyson-Schwinger, Bethe-Salpeter and Faddeev equations, which are employed to calculate the spectra of mesons, baryons and four-quark states. We discuss dynamical mass generation as a consequence of the spontaneous breaking of chiral symmetry, which is intertwined with the emergence of the light pions as Goldstone bosons of QCD. We highlight the importance of diquark correlations in the baryon sector, while for four-quark states such as the light scalar mesons and heavy exotics the dominant two-body clusters are typically mesons. We conclude with a brief discussion of hadron matrix elements like electromagnetic form factors and how vector-meson dominance is an automatic outcome of functional equations.

Keywords: Dynamical mass generation, Dyson-Schwinger and Bethe-Salpeter equations, Diquarks, Exotic hadrons, Form factors

Nomenclature

axWTI	Axialvector Ward-Takahashi identity
BSE	Bethe-Salpeter equation
DSE	Dyson-Schwinger equation
GMOR	Gell-Mann-Oakes-Renner
LHC	Large Hadron Collider
PCAC	Partially conserved axialvector current
PDG	Particle Data Group
QCD	Quantum chromodynamics
QFT	Quantum field theory

Objectives

- Understand how dynamical mass generation comes about and why the pion is so light.
- Explain the basic concepts behind Dyson-Schwinger, Bethe-Salpeter and Faddeev equations.
- Overview of baryon spectroscopy with three-quark and quark-diquark calculations.
- Exotic four-quark spectroscopy and the dynamical generation of resonances.
- Brief overview of hadron structure calculations with functional methods.

1 Introduction

The spectrum and structure of hadrons encodes a wealth of interesting phenomena. Hadrons are composites of quarks and gluons, the fundamental degrees of freedom in Quantum Chromodynamics (QCD) which is the theory of the strong interaction. Because quarks and gluons carry color, they are confined in hadrons and cannot be directly probed in experiments. Traditionally, hadrons are classified in mesons as quark-antiquark ($q\bar{q}$) states and baryons as composites of three valence quarks (qqq). However, nowadays we know that the situation is substantially more complex: There is experimental evidence for exotic hadrons like tetraquarks ($qq\bar{q}\bar{q}$) and pentaquarks ($qqqq\bar{q}$), and there could also be hybrid mesons with extra valence gluons or glueballs made of gluons only. Even our understanding of the nucleon is far from complete: Protons (uud) and neutrons (udd) consist of three light up and down quarks, whose masses sum up to only about 1% of the nucleon mass. Thus, the overwhelming remainder must be generated in QCD. This property of dynamical mass generation has to do with chiral symmetry, which is also responsible for the small masses of the pions as the lightest mesons.

Even though QCD is fully defined by its Lagrangian, extracting observables is much more complicated compared to the electroweak sector of the Standard Model. For example, suppose we want to calculate the scattering of two electrons (Møller scattering) in Quantum Electrodynamics. To do so, we just need to sum up the Feynman diagrams contributing to the process in the lowest orders of the electromagnetic coupling $\alpha_{em} = e^2/(4\pi) \approx 1/137$ and compare the resulting cross section with experiment. In QCD, this strategy does not work for two reasons. First, confinement means that a process like $q\bar{q} \rightarrow q\bar{q}$ scattering is not directly measurable, so one must find a passage to channel such processes to the observable world of hadrons. Second, perturbative expansions are only possible at large momenta, where the strong coupling α_s is small. At small momenta, α_s becomes large and perturbation theory is no longer applicable to calculate hadron properties — instead, one needs nonperturbative methods.

Nowadays, lattice QCD has become the primary tool to calculate hadron properties from first principles. There, one computes correlation functions from the QCD path integral. These have poles in momentum space corresponding to hadrons with masses m_i . The Fourier transform of a pole yields an exponential falloff $\sim e^{-m_i\tau}$ in Euclidean time τ , from where one can extract the hadron mass m_i (see e.g. [1]).

An alternative approach, which is also based on the path integral, is the one via functional methods. By taking functional derivatives of the path integral, the classical equations of motion (Klein-Gordon, Dirac, Maxwell equations) are converted into quantum equations of motion, which are the Dyson-Schwinger equations (DSEs) [2–7]. These are coupled integral equations which relate QCD's n -point correlation functions with each other. Fig. 1 shows exemplary DSEs for the two-point functions like the quark propagator and gluon propagator, three-point functions like the three-gluon vertex, and the list goes on. A similar method is the functional renormalization group, which leads to coupled integro-differential equations for the n -point functions [8–10]. So, instead of computing correlation functions directly from the path integral like in lattice QCD, one derives relations from the path integral to calculate them *from each other*. While the Lagrangian defines the classical field theory, the set of all n -point correlation functions defines the corresponding quantum field theory (QFT) completely.

Hadrons appear as poles in QCD's n -point functions. For example, the process $q\bar{q} \rightarrow q\bar{q}$ contains all possible meson poles. This is how hadron masses are extracted in lattice QCD, and the same is true for functional methods. As we will see in the following sections, one can derive Bethe-Salpeter equations (BSEs) which are valid at these poles. These are the QFT analogues of the Schrödinger equation in quantum mechanics. The n -point correlation functions then appear in the kernels of these equations. From a BSE one can calculate the mass of a hadron and its ‘wave function’ (the Bethe-Salpeter amplitude). Once the wave function is known, one can compute hadron matrix elements like form factors, scattering amplitudes and parton distributions.

In the following we discuss the basics of hadron spectroscopy and structure calculations with functional methods, along with a brief survey of some results obtained so far. We will frequently refer to the reviews [5, 11], where details and references to the literature can be found. We use Euclidean conventions throughout, which are collected in Appendix A of Ref. [5].

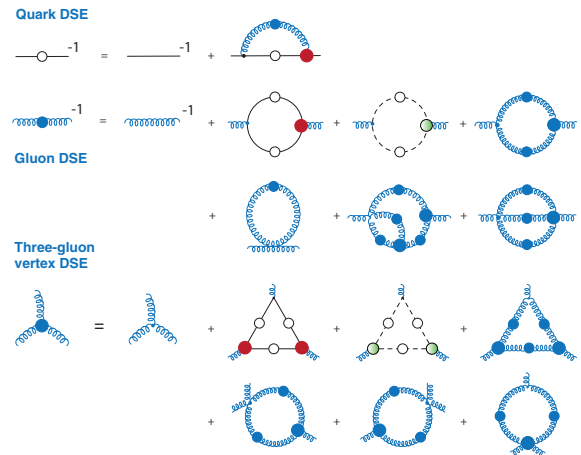


Fig. 1 Coupled Dyson-Schwinger equations for the quark propagator, gluon propagator and three-gluon vertex.

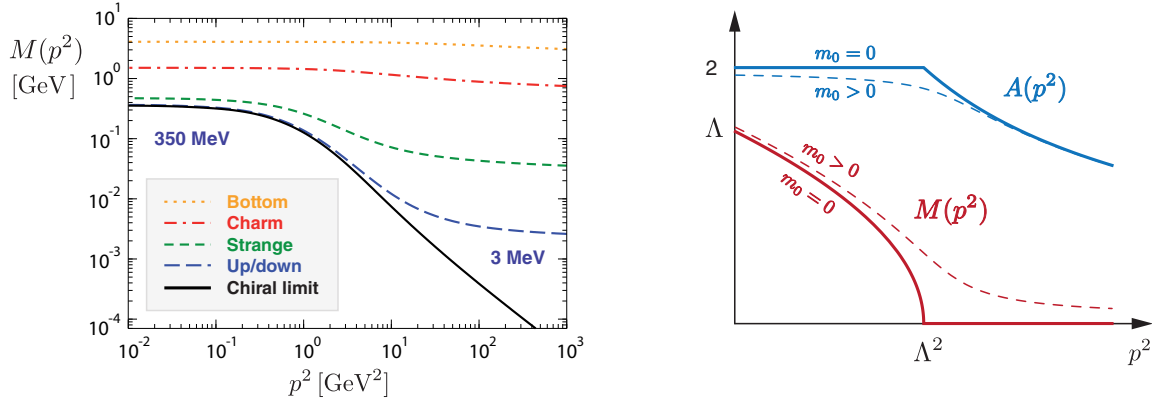


Fig. 2 Left: Quark mass function for different flavors obtained by solving the quark Dyson-Schwinger equation [5]. Right: Dressing functions of the quark propagator in the Munczek-Nemirovsky model, Eqs. (12–13).

2 Quarks

2.1 Dynamical mass generation

Light quarks are quite special because most of their mass is dynamically generated in QCD through their interactions with gluons. The light up and down quarks have current-quark masses of only about 2–5 MeV, which arise from the Higgs mechanism as external inputs to QCD. In contrast, the mass of a proton composed of uud is 938 MeV. This striking difference implies that nearly all the mass of the proton – and consequently the masses of nuclei, atoms, and the baryonic matter in the universe – must be generated within QCD itself. The phenomenon is called dynamical mass generation, and it can be understood through the dynamical breaking of chiral symmetry, a nonperturbative effect arising from the interactions of quarks and gluons which cause the quarks to gain mass.

Dynamical mass generation is visible in the quark propagator (among many other quantities), which is the two-point function

$$S_{\alpha\beta}(p) = \int d^4x e^{-ipx} \langle 0 | T \psi_\alpha(x) \bar{\psi}_\beta(0) | 0 \rangle \quad (1)$$

and therefore the basic object describing a quark in QCD. Here, ψ_α and $\bar{\psi}_\beta$ are the quark and antiquark fields, and T stands for time ordering. Because quarks are spin-1/2 particles, the most general form of the quark propagator $S(p)$ in momentum space according to Lorentz invariance is

$$S(p)^{-1} = A(p^2) (i\not{p} + M(p^2)) \Leftrightarrow S(p) = \frac{1}{A(p^2)} \frac{-i\not{p} + M(p^2)}{p^2 + M(p^2)^2} = -i\not{p} \sigma_v(p^2) + \sigma_s(p^2). \quad (2)$$

It depends on two dressing functions, $A(p^2)$ and the quark mass function $M(p^2)$, or equivalently the two dressing functions $\sigma_v(p^2)$ and $\sigma_s(p^2)$ as combinations of them. The variable p^2 can take any value $p^2 \in \mathbb{C}$, but in the following we are mainly interested in spacelike momenta $p^2 \in \mathbb{R}_+$. For a free spin-1/2 particle with mass m , the above would simplify to $A(p^2) = 1$, $M(p^2) = m$ and therefore

$$S(p) = \frac{-i\not{p} + m}{p^2 + m^2} \Leftrightarrow \sigma_v(p^2) = \frac{1}{p^2 + m^2}, \quad \sigma_s(p^2) = \frac{m}{p^2 + m^2}. \quad (3)$$

Switching on interactions, the masses and couplings in a quantum field theory become momentum-dependent. As shown in the left panel of Fig. 2, the effect is quite drastic for the quark mass function $M(p^2)$: At large momenta, $M(p^2)$ coincides with the current-quark mass m , while at small momenta it is much larger by several hundred MeV and thereby defines a ‘constituent-quark mass’, which is the relevant mass scale for the proton and other hadrons.

That this effect is due to the spontaneous breaking of chiral symmetry can be seen as follows. In the chiral limit, where the current-quark masses vanish, the QCD Lagrangian has a chiral symmetry $SU(N_f)_L \times SU(N_f)_R \simeq SU(N_f)_V \times SU(N_f)_A$, where N_f denotes the number of quark flavors. This is larger than the usual (vector) flavor symmetry $SU(N_f)_V$, which would be satisfied if all quark masses were identical. Collecting all quark flavors in an N_f -dimensional vector ψ , the symmetry operations read

$$SU(N_f)_V: \quad \psi' = e^{i \sum_a \varepsilon_a t_a} \psi, \quad SU(N_f)_A: \quad \psi' = e^{i \gamma_5 \sum_a \varepsilon_a t_a} \psi, \quad (4)$$

where the t_a are the $SU(N_f)$ generators ($a = 1 \dots N_f^2 - 1$) and the ε_a are the parameters of the global transformations. The axial $SU(N_f)_A$ symmetry only holds in the chiral limit and is explicitly broken if the quark masses are non-zero. Now, if chiral symmetry were preserved also at the quantum level, then all n -point correlation functions would be chirally symmetric. For the quark propagator this implies $\{\gamma_5, S(p)\} = 0$, which follows from plugging in the axial transformation (4) of the quark fields into Eq. (1). Using the decomposition (2), this yields $M(p^2) = 0$, in contrast to the result shown in Fig. 2. Apparently there must be some dynamical mechanism that generates a quark mass ‘out of nothing’, i.e., even in the chiral limit of vanishing current-quark masses.

4 Hadron physics with functional methods

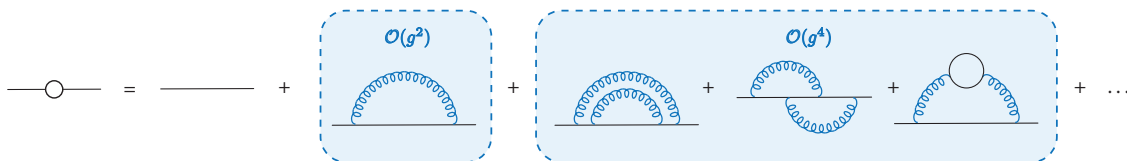


Fig. 3 Perturbative expansion of the quark propagator.

The fact that this effect is *nonperturbative* means that one cannot produce it at any order in perturbation theory, which is the standard tool to make a QFT useful in practice. When expanding the quark propagator in powers of g , as shown in Fig. 3, one generates all possible Feynman diagrams, where each comes with a power in the strong coupling $\alpha_s = g^2/(4\pi)$. If the coupling is small enough, one can stop the series after a few terms. For QCD this only works at large momenta, where α_s is small; this is what allows one to describe high-energy scattering processes. However, for small momenta α_s becomes large and perturbation theory fails. The ingredients of the perturbative expansion are the tree-level quark-gluon vertex $\sim i\gamma^\mu$ and the tree-level quark propagator, which in the chiral limit ($m = 0$) via Eq. (3) is given by $-i\cancel{p}/p^2$ (up to a renormalization constant). Now, because both quantities contain one γ -matrix, every possible perturbative diagram contains an odd number of γ -matrices. Thus, the trace of the quark propagator vanishes to all orders in perturbation theory! However, by Eq. (2) that trace is proportional to the quark mass function, which therefore vanishes in perturbation theory.

How can we generate a mass nonperturbatively? A simple analogue of the perturbative expansion is the geometric series

$$\sum_{n=0}^{\infty} x^n = \frac{1}{1-x} \quad \text{for } |x| < 1, \quad (5)$$

which converges only for $|x| < 1$. But suppose someone gave you the ‘nonperturbative’ equation

$$f(x) = 1 + xf(x) \quad \Leftrightarrow \quad f(x)^{-1} = 1 - x, \quad (6)$$

which has the solution $f(x) = 1/(1-x)$ for any x except $x = 1$. When inserting the l.h.s. into the r.h.s., then

$$f(x) = 1 + xf(x) = 1 + x + x^2 f(x) = 1 + x + x^2 + x^3 f(x) = \dots \quad (7)$$

is still ‘nonperturbative’ and exact at every step. In the geometric series, on the other hand, we dropped the last term which otherwise pulls the result back even if x becomes large, and this is what makes the perturbative expansion fail.

The analogues of Eq. (6) in QCD are the DSEs, which are the exact, non-perturbative quantum equations of motion in a QFT. The quark DSE is shown in the left panel of Fig. 4 and reads explicitly

$$S(p)^{-1} = Z_2(i\cancel{p} + m_0) + \Sigma(p), \quad \Sigma(p) = -\frac{4g^2}{3} Z_\Gamma \int \frac{d^4 q}{(2\pi)^4} i\gamma^\mu S(q) D^{\mu\nu}(k) \Gamma^\nu(l, k). \quad (8)$$

Here, $\Sigma(p)$ is the quark self-energy that depends on the gluon propagator $D^{\mu\nu}(k)$ with momentum $k = q - p$, the full quark-gluon vertex $g\Gamma^\mu(l, k)$ with relative momentum $l = (p + q)/2$ and total momentum k , and the tree-level vertex $g Z_\Gamma i\gamma^\mu$ with renormalization constant Z_Γ . The prefactor $4/3$ comes from the color trace, m_0 is the bare current quark mass that enters in the QCD Lagrangian, and Z_2 is the quark renormalization constant.

Note that the full quark propagator appears again inside the loop, so the DSE is an integral equation for $S(p)$. It has the structural form $f(x)^{-1} = 1 - x$ from Eq. (6), where $-x$ plays the role of the self-energy. Thus, if g is small one can expand $S(p)$ in a series like in Eq. (7) by reinserting the equation at every instance where the quark propagator appears inside the loop, doing the same for the gluon propagator and quark-gluon vertex, and stop after a few terms — this reproduces the perturbative series for the quark propagator shown in Fig. 3. However, if the coupling is large we have no choice but to solve the equation directly.

2.2 An illustrative model

At this stage you might be tempted to throw your hands in the air and follow the standard textbook advice, which portrays perturbation theory as intuitive and easy to grasp while nonperturbative phenomena are something more obscure and best left to specialists. However, the quark DSE serves as a hands-on example of how nonperturbative properties can be understood with surprising ease. There are simple analytically solvable models that capture the basic features in Fig. 2 [5, 12]. An illustrative example is the Munczek-Nemirovsky model [13], where the quark-gluon vertex in Eq. (8) is approximated by a bare vertex, $\Gamma^\nu(l, k) = i\gamma^\nu$, and the gluon propagator by a δ distribution, with a scale Λ to ensure the correct dimension:

$$\frac{4}{3} \frac{g^2}{(2\pi)^4} D^{\mu\nu}(k) \rightarrow \Lambda^2 \delta^4(k) \delta^{\mu\nu}. \quad (9)$$

Shifting the integration momentum $d^4 q \rightarrow d^4 k$, the integral can be solved analytically, so there are no loop divergences and one can set the renormalization constants $Z_2 = Z_\Gamma = 1$. The DSE then turns into

$$S(p)^{-1} = i\cancel{p} + m_0 + \Lambda^2 \gamma^\mu S(p) \gamma^\mu. \quad (10)$$

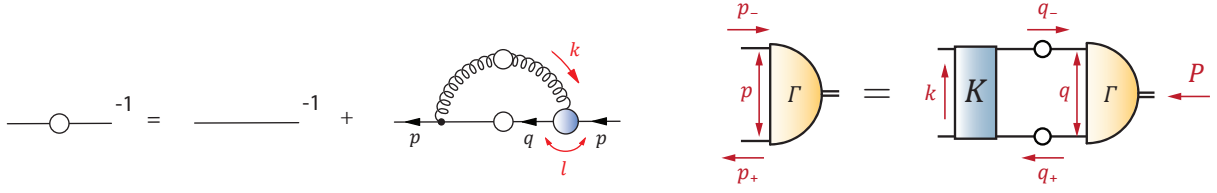


Fig. 4 Left: Quark DSE from Eq. (8). The lines with circles denote the full quark propagator, and the self-energy depends on the full gluon propagator and quark-gluon vertex. Right: Bethe-Salpeter equation (19) for a meson.

Plugging in the decomposition (2) yields two algebraic equations for $A(p^2)$ and $M(p^2)$:

$$A(p^2) = 1 + \frac{2\Lambda^2}{A(p^2)(p^2 + M(p^2)^2)}, \quad A(p^2)M(p^2) = m_0 + 2M(p^2) \frac{2\Lambda^2}{A(p^2)(p^2 + M(p^2)^2)}. \quad (11)$$

In the chiral limit $m_0 = 0$, the chiral-symmetry preserving solution $M(p^2) = 0$ is still possible and yields a quadratic equation for $A(p^2)$, whose solution is

$$A(p^2) = \frac{1}{2} \left(1 + \sqrt{1 + \frac{8\Lambda^2}{p^2}} \right). \quad (12)$$

Here we picked the positive branch that reproduces the correct perturbative behavior $A(p^2) = 1$. However, there is also a chiral-symmetry breaking solution with $M(p^2) \neq 0$. Plugging the first equation above into the second yields

$$A(p^2) = 2, \quad M(p^2) = \sqrt{\Lambda^2 - p^2}. \quad (13)$$

The two solutions are connected at $p^2 = \Lambda^2$, as shown in the right panel of Fig. 2. When switching on the current-quark mass $m_0 \neq 0$, the solution becomes more cumbersome but the curves are now smooth. Note the analogy with the spontaneous magnetization of a magnet below a critical temperature if p^2 is replaced by temperature, $M(p^2)$ by magnetization and the current-quark mass m_0 by an external magnetic field. Loosely speaking, below a critical momentum $p^2 = \Lambda^2$, QCD dynamically generates a quark mass $M(p^2)$ even if the quarks in the QCD Lagrangian are massless. In more realistic DSE solutions, there is no sharp phase transition in the chiral limit and one instead finds the behavior in the left panel of Fig. 2.

How do we know the gluon propagator and quark-gluon vertex, which appear as inputs in the quark DSE? These quantities satisfy their own DSEs, which depend again on the quark propagator but also on higher n -point functions, so one arrives at a coupled system of equations which needs to be solved (Fig. 1). Alternatively, if the gluon propagator and quark-gluon vertex are sufficiently well known, one can make a combined ansatz for them (an ‘effective interaction’) and solve the quark DSE as a standalone equation. The second route has turned out especially useful in combination with hadron physics applications, to which we will turn in Sec. 3.

2.3 About renormalization

Before doing so, it is worthwhile to briefly discuss the issue of renormalization, because the quark DSE illustrates the basic steps that are similar for other n -point functions. To this end, let us write the quark self-energy as $\Sigma(p) = i\not{p} \Sigma_A(p^2) + \Sigma_M(p^2)$, so that by Eq. (2) the quark DSE turns into two coupled scalar equations for $A(p^2)$ and $M(p^2)$:

$$A(p^2) = Z_2 + \Sigma_A(p^2), \quad M(p^2)A(p^2) = Z_2 m_0 + \Sigma_M(p^2). \quad (14)$$

The self-energy integrals are logarithmically UV-divergent, so they must first be regularized, e.g., by integrating up to a finite cutoff. In the renormalization step we set two boundary conditions for the integral equations by demanding

$$A(\mu^2) \stackrel{\dagger}{=} 1, \quad M(\mu^2) \stackrel{\dagger}{=} m. \quad (15)$$

The second condition introduces the renormalized current-quark mass m for a given quark flavor at some arbitrary renormalization scale $p^2 = \mu^2$. The first condition $A(\mu^2) = 1$ is arbitrary and merely induces a renormalization of $A(p^2)$; if we chose another value this would not affect any observable. Eq. (14) then fixes the bare parameters Z_2 and m_0 , which are divergent if the cutoff is sent to infinity:

$$Z_2 = 1 - \Sigma_A(\mu^2), \quad m_0 = \frac{m - \Sigma_M(\mu^2)}{1 - \Sigma_A(\mu^2)}. \quad (16)$$

Plugging this back into Eq. (14) yields the final form of the DSEs:

$$A(p^2) = 1 + \Sigma_A(p^2) - \Sigma_A(\mu^2), \quad M(p^2)A(p^2) = m + \Sigma_M(p^2) - \Sigma_M(\mu^2). \quad (17)$$

We see that the boundary conditions in Eq. (15) led to subtracted equations at the renormalization point; this is called a momentum-subtraction (MOM) scheme. Due to this subtraction, all divergences cancel and the dressing functions $A(p^2)$ and $M(p^2)$ are finite. These

6 Hadron physics with functional methods

equations can be solved iteratively: start with some guess for $A(p^2)$ and $M(p^2)$ (e.g., set them to 1), calculate $\Sigma_A(p^2)$ and $\Sigma_M(p^2)$ from Eq. (8), determine $\Sigma_A(\mu^2)$ and $\Sigma_M(\mu^2)$ and correspondingly Z_2 from Eq. (16), and arrive at new values for $A(p^2)$ and $M(p^2)$, which enter in the self-energy in the next step. The procedure is then repeated until convergence.

In the renormalization process we traded the cutoff dependence for a dependence on the renormalization point μ , so that $A(p^2)$ now also depends on μ . The mass function $M(p^2)$, on the other hand, is renormalization-group invariant: After having solved the quark DSE, one can read off $M(p^2 = \mu'^2) = m'$ at another value μ' , use this as the new renormalization condition instead of Eq. (15) and solve the equations anew. The resulting mass function is the same as before (so it does not depend on μ), whereas $A(p^2)$ differs by a multiplicative constant. Note also that the renormalization scale μ is completely arbitrary; one may choose a very large value $\mu = 100$ GeV or just as well renormalize at $\mu = 0$.

3 Mesons

The spontaneous breaking of chiral symmetry has important consequences for hadron physics. On the one hand, the large dynamical quark mass in Fig. 2 is the effective mass that enters in mesons and baryons as bound states of valence quarks. Without it, the spectrum of hadrons would look very different or they would not even be able to form. On the other hand, the spontaneous breaking of a global symmetry leads to massless Goldstone bosons in the spectrum. In QCD these are the pseudoscalar mesons, in particular the three pions whose masses of about 140 MeV are much smaller than the masses of other hadrons (which are of the order of 1 GeV). Therefore, the pion plays a special role in QCD: It is a bound state of a valence quark and antiquark but at the same time the (pseudo-)Goldstone boson of spontaneous chiral symmetry breaking, whose mass would be exactly zero in the chiral limit.

3.1 Bethe-Salpeter equation

These features are explicit in the Bethe-Salpeter equation (BSE) for the pion [14]. BSEs can be viewed as the quantum field-theoretical analogues of the Schrödinger equation in quantum mechanics: They are eigenvalue equations which allow one to calculate the spectrum and wave functions of hadrons. Here the word ‘analogue’ is important: Because the Poincaré group is not compact (it contains Lorentz boosts), its unitary representations must be infinite-dimensional. This is why quantum mechanics is not enough to describe special relativity and one should employ QFT, which provides unitary representations on the infinite-dimensional Fock space and thus a probability interpretation. The Bethe-Salpeter wave function, on the other hand, is defined as

$$[i\Psi(p, P)]_{\alpha\beta} = \int d^4x e^{-ipx} \langle 0 | \mathbb{T} \psi_\alpha(x) \bar{\psi}_\beta(0) | P, n \rangle, \quad (18)$$

where P is the total onshell momentum of the hadron ‘ n ’ defined by quantum numbers like spin J , parity P , flavor, etc. Because the quark spinors transform under finite-dimensional (Dirac) representations of the Lorentz group, so does the Bethe-Salpeter wave function. As such, it does not have a direct probabilistic interpretation like the wave functions in quantum mechanics. Nevertheless, it encodes the internal structure of a hadron and enters in observables through matrix elements like, e.g., form factors and parton distributions.

The general form of the BSE for a meson made of a valence quark and antiquark is shown in the right panel of Fig. 4 and reads

$$[\Gamma(p, P)]_{\alpha\beta} = \int \frac{d^4q}{(2\pi)^4} [\mathbf{K}(p, q, P)]_{\alpha\gamma, \delta\beta} [S(q_+) \Gamma(q, P) S(q_-)]_{\gamma\delta}. \quad (19)$$

The Bethe-Salpeter amplitude $\Gamma(p, P)$ is defined as the wave function $\Psi(p, P) = S(p_+) \Gamma(q, P) S(p_-)$ without external quark propagator legs. The quark-antiquark kernel $\mathbf{K}(p, q, P)$ contains all possible two-particle irreducible interactions between quark and antiquark, i.e., those that are not already generated by the iteration. $S(q_\pm)$ is again the full quark propagator from Eq. (2). There are further color and flavor indices stemming from the quark fields in Eq. (18), but we absorbed them in the Greek subscripts which are therefore multi-indices in Dirac, color and flavor space.

How is the BSE derived? This is closely related to the way how bound states appear in QFT in general. A QFT is fully specified by its (infinitely many) n -point correlation functions. Bound states appear as poles in these correlation functions. Take for example the quark-antiquark four-point function describing $q\bar{q} \rightarrow q\bar{q}$ scattering, which is shown in Fig. 5:

$$\mathbf{G}_{\alpha\beta\gamma\delta}(x_1, x_2, x_3, x_4) = \langle 0 | \mathbb{T} \psi_\alpha(x_1) \bar{\psi}_\beta(x_2) \psi_\gamma(x_3) \bar{\psi}_\delta(x_4) | 0 \rangle. \quad (20)$$

Inserting a complete set of states produces meson poles, because a composite operator $\psi\bar{\psi}$ can produce color singlet quantum numbers ($\mathbf{3} \otimes \bar{\mathbf{3}} = \mathbf{1} \oplus \mathbf{8}$). At a given pole, the four-point function factorizes and defines the Bethe-Salpeter wave function as the residue at the pole:

$$\mathbf{G}(p, q, P) \xrightarrow{p^2 \rightarrow -m_n^2} \frac{\Psi(p, P) \bar{\Psi}(q, P)}{P^2 + m_n^2}. \quad (21)$$

The proof of this relation can be found, e.g., in Weinberg’s book [15]. In momentum space, the four-point function depends on three independent momenta (e.g., the relative momenta p , q and the total momentum P), and it has poles whenever the total momentum goes onshell ($P^2 = -m_n^2$). Actually, Eq. (21) can also be used to *define* the wave function — this is useful when the definition (18) is no longer applicable, as in the case of unstable resonances where $|P, n\rangle$ is not an asymptotic state and the mass m_n becomes complex.

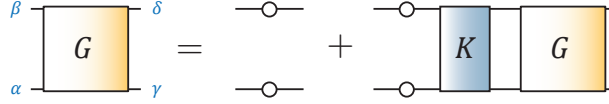


Fig. 5 Scattering equation for the quark-antiquark four-point function.

The fact that composite states appear as poles in n -point functions is a central feature of QFT: This is what makes it possible to extract hadron properties experimentally, namely from bumps and peaks in experimental cross sections. It is also the underlying basis for theoretical treatments of bound states in QFT such as e.g. lattice calculations, effective field theories and functional methods.

The actual derivation of the BSE in Eq. (19) goes as follows. The four-point function \mathbf{G} satisfies the scattering equation shown in Fig. 5, which has the structural form

$$\mathbf{G} = \mathbf{G}_0 + \mathbf{G}_0 \mathbf{K} \mathbf{G}. \quad (22)$$

Here, every multiplication stands for a four-dimensional momentum integration $\int d^4 q_i / (2\pi)^4$, and \mathbf{G}_0 is the disconnected part of \mathbf{G} , i.e., the product of quark and antiquark propagators. \mathbf{K} is the $q\bar{q}$ irreducible kernel, which contains all interactions between quark and antiquark that do not fall apart by cutting two quark lines, i.e., those that are not already generated by the iteration $\mathbf{G} = \mathbf{G}_0 + \mathbf{G}_0 \mathbf{K} \mathbf{G}_0 + \mathbf{G}_0 \mathbf{K} \mathbf{G}_0 \mathbf{K} \mathbf{G}_0 + \dots$. Now, at a given meson pole location the four-point function \mathbf{G} satisfies Eq. (21). Comparing residues on both sides of the scattering equation, and because \mathbf{G}_0 does not have meson poles, we arrive at the homogeneous BSE $\Psi = \mathbf{G}_0 \mathbf{K} \Psi$ which holds at the pole. With $\Psi = \mathbf{G}_0 \Gamma$, this can also be expressed in terms of the Bethe-Salpeter amplitude as in Eq. (19), $\Gamma = \mathbf{K} \mathbf{G}_0 \Gamma$.

A few remarks are in order:

- It is useful to define the scattering matrix \mathbf{T} as the connected part of $\mathbf{G} = \mathbf{G}_0 + \mathbf{G}_0 \mathbf{T} \mathbf{G}_0$, so that Eq. (22) turns into the scattering equation $\mathbf{T} = \mathbf{K} + \mathbf{K} \mathbf{G}_0 \mathbf{T}$. Because any pole in \mathbf{G} must also show up in \mathbf{T} , Eq. (21) holds for \mathbf{T} alike if Ψ is replaced by Γ . This yields again the homogeneous BSE $\Gamma = \mathbf{K} \mathbf{G}_0 \Gamma$.
- The homogeneous BSE is an eigenvalue equation. If we label the ground state in a given J^{PC} channel by $n = 0$ and the excited states by $n \geq 1$, we have

$$\mathbf{K} \mathbf{G}_0 \Gamma^{(n)} = \lambda^{(n)} \Gamma^{(n)}. \quad (23)$$

That is, if a given eigenvalue $\lambda^{(n)}$ satisfies $\lambda^{(n)} = 1$, we have found a pole in \mathbf{G} and \mathbf{T} . This is also obvious when we write the scattering equations in their inverse forms, $\mathbf{G}^{-1} = \mathbf{G}_0^{-1} - \mathbf{K}$ and $\mathbf{T}^{-1} = \mathbf{K}^{-1} - \mathbf{G}_0$. A pole in \mathbf{G} and \mathbf{T} implies a zero in \mathbf{G}^{-1} and \mathbf{T}^{-1} , which in turn requires an eigenvalue for $\mathbf{K} \mathbf{G}_0$ which is 1.

- In practice, it is useful to work out the tensor decomposition of the amplitude $\Gamma(p, P)$ in order to obtain Lorentz-invariant equations for its dressing functions. The pion amplitude has a Dirac, flavor and color part:

$$\Gamma(p, P) = (f_1 + f_2 i \not{P} + f_3 (p \cdot P) i \not{p} + f_4 [\not{p}, \not{P}]) \gamma_5 \otimes \text{Flavor} \otimes \text{Color}. \quad (24)$$

The first part is a matrix in Dirac space which depends on four linearly independent Dirac tensors. We denoted their dressing functions by $f_i(p^2, z, P^2 = -m_\pi^2)$, where $z = \hat{p} \cdot \hat{P}$ is the angular variable and a hat denotes a normalized unit vector, $\hat{p}^\mu = p^\mu / \sqrt{p^2}$. After taking Dirac, color and flavor traces, the BSE (19) assumes the Lorentz-invariant form

$$\lambda^{(n)}(P^2) f_i^{(n)}(p^2, z, P^2) = \int_0^\infty dq^2 \int_{-1}^1 dz' K_{ij}(p^2, q^2, z, z', P^2) f_j^{(n)}(q^2, z', P^2). \quad (25)$$

If we further discretize the variables p^2 and z , this becomes a matrix-vector eigenvalue equation whose outcomes are the eigenvalues $\lambda^{(n)}(P^2)$ and corresponding eigenvectors. As shown in Fig. 6, if an eigenvalue crosses the line 1, this implies a pole in the scattering matrix and thus a physical solution.

- The homogeneous BSE holds for bound states and resonances alike. The pole condition (21) does not care if the mass m_n is real or complex. For a bound state, the condition $\lambda^{(n)}(P^2 = -m_n^2) = 1$ has a solution for real m_n , while for a resonance the solution lies in the complex plane on a higher Riemann sheet. Then, by solving the BSE for complex values of P^2 on the first sheet, the resulting eigenvalues $\lambda^{(n)}(P^2)$ can be analytically continued to the second sheet to solve the pole condition, see e.g. [16] for examples. In practice, solving for complex P^2 can be technically challenging and may require contour deformations.

3.2 Chiral properties of the pion

What does the kernel \mathbf{K} look like? So far we only know that it must be two-particle irreducible, because this is how the scattering equation (22) was defined. Clearly, somehow \mathbf{K} must be aware of chiral symmetry to produce a massless pion in the chiral limit. To this end, let us make a brief detour and sketch the chiral properties of the pion (see [5, 14] for details). Consider the axialvector and pseudoscalar currents, whose matrix elements define the pion's electroweak decay constant f_π and its 'pseudoscalar decay constant' r_π :

$$\begin{aligned} j_5^\mu(x) &= Z_2 \bar{\psi}(x) i \gamma^\mu \gamma_5 \psi(x), & \langle 0 | j_5^\mu(x) | P \rangle &= \langle 0 | j_5^\mu(0) | P \rangle e^{ix \cdot P} = i f_\pi P^\mu e^{ix \cdot P}, \\ j_5(x) &= Z_2 Z_m \bar{\psi}(x) i \gamma_5 \psi(x), & \langle 0 | j_5(x) | P \rangle &= \langle 0 | j_5(0) | P \rangle e^{ix \cdot P} = r_\pi e^{ix \cdot P}. \end{aligned} \quad (26)$$

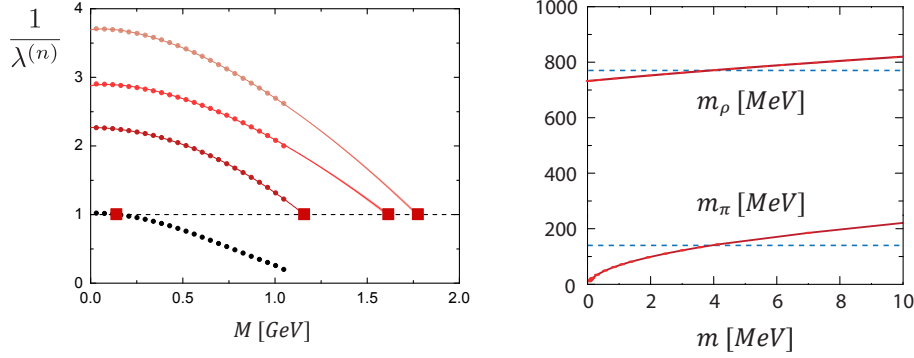


Fig. 6 Left: inverse eigenvalues $\lambda^{(n)}(p^2 = -M^2)$ of the pion BSE as functions of M [17]. The points are numerical results and the bands are fits. Whenever an eigenvalue crosses the line 1, one has found a physical solution $M = m_n$ (red squares). The calculation stops at $M \approx 1.1$ GeV because for larger values one would need to circumvent quark singularities in the integrand. Right: pion and ρ -meson masses obtained from their Bethe-Salpeter equations and plotted over the current-quark mass m (which is an input in the quark DSE, Eq. (15)). The horizontal dashed lines are the experimental values [5]. The pion mass satisfies the GMOR relation (31).

Here we denoted the pion state by $|P\rangle$, Z_2 is the quark renormalization constant, and Z_m is the quark mass renormalization constant (the bare and renormalized masses are related by $m_0 = Z_m m$). One can see from Eq. (18) that these are just the four-momentum integrals over the Bethe-Salpeter wave function $\Psi(p, P)$, once taking the trace with $\gamma^\mu \gamma_5$ and once with γ_5 :

$$f_\pi P^\mu = Z_2 \int \frac{d^4 p}{(2\pi)^4} \text{Tr} \{i\gamma_5 \gamma^\mu \Psi(p, P)\}, \quad r_\pi = Z_2 Z_m \int \frac{d^4 p}{(2\pi)^4} \text{Tr} \{\gamma_5 \Psi(p, P)\}. \quad (27)$$

Once the pion wave function is known from its BSE, it is thus an easy task to calculate f_π .

Now consider the PCAC relation $\partial_\mu j_5^\mu = 2m j_5$, which follows from the Noether theorem and reflects the explicit breaking of the axialvector symmetry in Eq. (4) away from the chiral limit. Plugged into Eq. (26), we immediately find the relation

$$f_\pi m_\pi^2 = 2m r_\pi, \quad (28)$$

which is valid for all current-quark masses. In particular, this implies $f_\pi m_\pi^2 = 0$ in the chiral limit. So, if one can show that the pion decay constant f_π does *not* vanish in the chiral limit, then m_π must be zero.

The right place to look for such a relation is the axialvector Ward-Takahashi identity (axWTI), which is the PCAC relation evaluated for the three-point functions $\langle 0 | T \psi_\alpha(x) \bar{\psi}_\beta(y) j_5^\mu(z) | 0 \rangle$ and $\langle 0 | T \psi_\alpha(x) \bar{\psi}_\beta(y) j_5(z) | 0 \rangle$. These quantities have pion poles, whose residues are proportional to the pion amplitude $\Gamma(p, P)$. However, in the axWTI these poles cancel each other and one finds the chiral-limit relation

$$f_\pi \Gamma(p, 0) = A(p^2) M(p^2) \gamma_5, \quad (29)$$

where $A(p^2)$ and $M(p^2)$ are the quark dressing functions from Sec. 2. If chiral symmetry is dynamically broken and hence $M(p^2) \neq 0$, then the r.h.s. of this equation is nonzero, so also f_π cannot vanish in the chiral limit. Eq. (28) then entails $m_\pi = 0$ in the chiral limit. In other words, we just proved the Goldstone theorem! Note that by Eq. (29) the pion amplitude in the chiral limit is already determined by the quark propagator, so in the chiral limit the pion BSE and quark DSE are equivalent.

Finally, if we take the trace of Eq. (29) with $S(p) \gamma_5 S(p)$ and compare with (27), we obtain $f_\pi r_\pi = -\langle \bar{\psi} \psi \rangle / N_f$ in the chiral limit, where the quark condensate is the trace over the quark propagator:

$$-\frac{\langle \bar{\psi} \psi \rangle}{N_f} = Z_2 Z_m N_c \int \frac{d^4 p}{(2\pi)^4} \text{Tr} S(p) = Z_2 Z_m \frac{N_c}{(2\pi)^2} \int d^2 p \frac{p^2}{A(p^2)} \frac{M(p^2)}{p^2 + M(p^2)^2}. \quad (30)$$

Therefore, also the quark condensate is directly related to the quark mass function. Plugged into Eq. (28), this returns the Gell-Mann-Oakes-Renner (GMOR) relation, which says that near the chiral limit the squared pion mass is proportional to the current-quark mass:

$$f_\pi^2 m_\pi^2 = -2m \langle \bar{\psi} \psi \rangle / N_f. \quad (31)$$

3.3 Bethe-Salpeter kernel

The relations so far are exact. This implies that the pion obtained from the BSE is automatically massless in the chiral limit if (a) the BSE kernel satisfies chiral symmetry through the axWTI, and (b) chiral symmetry is dynamically broken such that $M(p^2) \neq 0$ in the chiral limit. As we saw in Sec. 2, the condition (b) is automatic in the DSE. Concerning (a), the axWTI can be rewritten as a consistency relation between the BSE kernel and the quark propagator, which must be satisfied by any practical truncation.

In principle one can derive the kernel from the quantum effective action, which leads to a systematic expansion in powers of loops and powers of n -point functions. The leading term in such an expansion is the rainbow-ladder truncation, which amounts to a gluon exchange between quark and antiquark. Here the quark-gluon vertex is reduced to its leading tensor $i\gamma^\mu$, and its dressing functions is combined with

that of the gluon propagator into an effective interaction $\alpha(k^2)$ which depends on the gluon momentum k only:

$$\mathbf{K}_{\alpha\gamma,\delta\beta}(p, q, P) = Z_2^2 \frac{4\pi\alpha(k^2)}{k^2} (\mathbf{t}_a)_{AC} (\mathbf{t}_a)_{DB} (i\gamma^\mu)_{\alpha\gamma} T_k^{\mu\nu} (i\gamma^\nu)_{\delta\beta}. \quad (32)$$

This automatically satisfies the axWTI and thus the chiral symmetry constraints. Z_2 is the quark renormalization constant, k^μ the gluon momentum, $T_k^{\mu\nu} = \delta^{\mu\nu} - k^\mu k^\nu / k^2$ the transverse projector for Landau gauge, and $\mathbf{t}_a = \lambda_a / 2$ are the generators of $SU(3)_c$ in the fundamental representation (the λ_a are the eight Gell-Mann matrices).

A popular ansatz for the effective interaction $\alpha(k^2)$ is the Maris-Tandy model [18], $\alpha(k^2) = \pi\eta^7 x^2 e^{-\eta^2 x} + \alpha_{UV}(x)$ with $x = k^2/\Lambda^2$. Here the second term $\alpha_{UV}(x)$ ensures the correct perturbative behavior at large momenta but is otherwise not important. The relevant term is the first one, which effectively depends on only one parameter, namely the scale $\Lambda = 0.72$ GeV that is chosen to reproduce the experimental pion decay constant $f_\pi \approx 92$ MeV. If one varies the shape parameter η within a certain range, the shape of the interaction may look very different, but many observables calculated with it are insensitive to this change. For this reason, also other forms of $\alpha(k^2)$ proposed in the literature lead to very similar results for observables [19].

With this one has all the tools ready to do spectroscopy calculations. The right panel in Fig. 6 shows the pion and ρ mass obtained from their respective BSEs as a function of the current-quark mass, which is an input to the quark DSE, Eq. (15). One can see that the GMOR relation (31) for the pion mass holds, $m_\pi \sim \sqrt{m}$. The pion mass vanishes in the chiral limit, while the ρ mass does not. Both features are direct consequences of dynamical chiral symmetry breaking and the associated dynamical mass generation.

The DSE/BSE approach using rainbow-ladder has been used for many practical calculations: masses and decay constants of light, heavy and heavy-light mesons; electromagnetic and transition form factors of mesons; parton distribution functions for pions and kaons; scattering amplitudes like $\pi\pi \rightarrow \pi\pi$, $\gamma\pi \rightarrow \pi\pi$, etc; see e.g. [4, 5, 20] and references therein. Also three- and four-quark states have been successfully calculated in this approach, as we will see in Sections 4 and 5. As stated above, the only relevant parameters are the scale Λ , which is fixed by f_π , and the current-quark masses which are fixed by certain meson masses — like in Fig. 6, where one can set the light u/d mass by the experimental pion mass (horizontal dashed line). In many cases this leads to predictions that lie within $\lesssim 5 \dots 10\%$ of experimental results. Notable exceptions are scalar and axialvector mesons (we will say more about scalar mesons in Sec. 5), some properties of heavy-light mesons (which can be improved [21] by feeding information on the quark propagator back into $\alpha(k^2)$), and the radial excitations in various J^{PC} channels. Obviously, rainbow-ladder is not full QCD, but it is a very useful starting point for a wide array of applications. It is also the turning point between QCD modelling and a systematic expansion in QCD's n -point functions, for which one must solve coupled systems of DSEs. Such investigations beyond rainbow-ladder are ongoing, see e.g. [5, 22–25].

3.4 An illustrative model (continued)

To conclude this section and illustrate some features in the chiral limit, let us again employ the toy model from Eq. (13). Plugging it into the quark condensate (30), with $M(p^2) = 0$ for $p^2 > \Lambda^2$, yields for a single flavor (e.g., an up quark)

$$-\langle \bar{u}u \rangle = \frac{N_c}{(2\pi)^2} \int_0^{\Lambda^2} dp^2 p^2 \frac{\sqrt{\Lambda^2 - p^2}}{2\Lambda^2} = \frac{2}{15} \frac{N_c}{(2\pi)^2} \Lambda^3. \quad (33)$$

Setting $\Lambda = 1$ GeV returns a reasonable value for the condensate: $-\langle \bar{u}u \rangle \approx (220 \text{ MeV})^3$. Concerning the BSE, in the chiral limit we can drop the dependence on the total momentum because the onshell pion satisfies $P^2 = 0$ and thus $P^\mu = 0$, so the amplitude has only one tensor $\Gamma(p) = f_1(p^2) \gamma_5$. Using the rainbow-ladder truncation (32) with the δ -distribution (9), the BSE at $P^2 = 0$ turns into

$$\Gamma(p) = \frac{4g^2}{3} \int \frac{d^4q}{(2\pi)^4} i\gamma^\mu S(q) \Gamma(q) S(q) i\gamma^\nu D^{\mu\nu}(k) \rightarrow -\Lambda^2 \gamma^\mu S(p) \Gamma(p) S(p). \quad (34)$$

If the amplitude is non-zero, $f_1(p^2)$ drops out from both sides of the equation and we obtain

$$1 = \Lambda^2 \gamma^\mu \gamma_5 S(p) \gamma_5 S(p) \gamma^\mu = \Lambda^2 \gamma^\mu S(-p) S(p) \gamma^\mu = \frac{4\Lambda^2}{A(p^2)^2 (p^2 + M(p^2)^2)}, \quad (35)$$

which is satisfied by Eq. (13). In other words, the BSE has eigenvalue 1 at $P^2 = 0$. As advertised, the pion obtained from the BSE in the chiral limit is automatically massless because the kernel respects chiral symmetry. Although in this simple model the BSE does not tell us what $f_1(p^2)$ itself looks like, we already know from Eq. (29) that $f_1(p^2) = A(p^2)M(p^2)/f_\pi$ must hold generally. This can be plugged back into Eq. (27) to get an expression for f_π in the chiral limit, which is known as the Pagels-Stokar formula [26]:

$$f_\pi^2 = \frac{N_c Z_2}{4\pi^2} \int dp^2 p^2 \frac{M(p^2)}{A(p^2)} \frac{1}{(p^2 + M(p^2)^2)^2} \left(M(p^2) - \frac{p^2}{4} \frac{dM(p^2)}{dp^2} \right). \quad (36)$$

The formula is not exact because f_2 , f_3 and f_4 in Eq. (24) do not vanish in the chiral limit, only P^μ does; but since they are all (strongly) suppressed compared to f_1 it is a very good approximation. In the Munczek-Nemirovsky model, we obtain

$$f_\pi = \sqrt{\frac{N_c}{2}} \frac{\Lambda}{4\pi}. \quad (37)$$

With $\Lambda = 1$ GeV this gives $f_\pi = 97$ MeV, which is again in the right ballpark. Finally, combining the results for f_π and $\langle \bar{u}u \rangle$, the GMOR relation (31) turns into $m_\pi^2 = \frac{32}{15} \Lambda m \approx 2\Lambda m$.

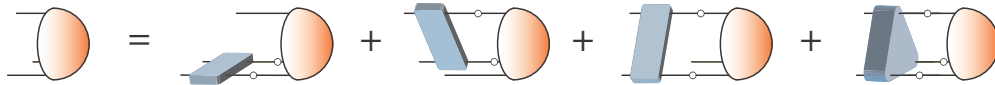


Fig. 7 Three-quark Faddeev equation with two- and three-body irreducible kernels.

4 Baryons

The proton is the only truly stable hadron. As such, it is a central ingredient in hadron structure experiments: from elastic and deep inelastic ep scattering to pp and $p\bar{p}$ reactions, $N\pi$ scattering, pion photo- and electroproduction, nucleon Compton scattering and more. Searches for physics beyond the Standard Model are usually also performed on protons and nuclei, which requires a precise understanding of the hadron physics background. The proton has a mass of almost 1 GeV, but the current quarks only contribute 2–5 MeV each. We argued that dynamical mass generation can explain such discrepancies, as exemplified in Fig. 6 for the ρ meson. Does the same apply for the proton?

The study of baryons also does not stop at the proton. The nucleon and Δ excitation spectra have been subject to many investigations in quark models, and new photo- and electroproduction experiments have added several new states to the PDG [27–32]. Especially interesting are also hyperons, i.e., baryons with strange quarks. Compared to light baryons, the experimentally known hyperon spectrum is still rather sparse even though it houses many interesting questions. Hyperons are important for hypernuclei and neutron stars, and the flavor-singlet $\Lambda(1405)$ made of uds is the prime candidate for a five-quark admixture in the light baryon sector [33]. In recent years, much experimental progress has also been made for charmed baryons where several new states have been found at LHCb [34].

4.1 Baryons made of three valence quarks

The three-body BSE is the covariant Faddeev equation shown in Fig. 7. In this case, the kernel is a sum of permuted two-quark irreducible kernels plus a three-quark irreducible kernel. It turns out that the leading three-body force, which is the three-gluon vertex connecting all three quark legs, vanishes by the color trace. This is simply due to the relation

$$f_{abc} (t_a)_{FM} (t_b)_{GN} (t_c)_{HR} \varepsilon_{MNR} = 0, \quad (38)$$

where f_{abc} is the color factor of the three-gluon vertex, the $SU(3)$ generators t_a belong to the quark-gluon vertices, and ε_{MNR} is the color wave function of the baryon. Of course, this does not prevent the appearance of higher n -point functions in the three-body kernel, like quark-two-gluon or four-gluon vertices, but the simplest option is discarded. This seems to point towards two-body correlations as the dominant forces in baryons. Neglecting the three-body kernel, the Faddeev equation can then be solved using the very same setup as in the meson sector, in particular with the same two-body kernel.

The main complication arises from the structure of the wave functions, which are much richer compared to the case of mesons in Eq. (24). For a baryon with spin $J = 1/2$, the Faddeev amplitude reads

$$\Gamma(p, q, P)_{\alpha\beta\gamma\delta} = \sum_{i=1}^{64} f_i(p^2, q^2, p \cdot q, p \cdot P, q \cdot P, P^2) \tau_i(p, q, P)_{\alpha\beta\gamma\delta} \otimes \text{Flavor} \otimes \varepsilon_{ABC}. \quad (39)$$

It has four Dirac indices, three for the valence quarks and one for the nucleon. This leads to 64 Dirac tensors for baryons with spin $J = 1/2$ and 128 tensors for $J = 3/2$. Furthermore, the amplitude is a four-point function, so it depends on three independent momenta, e.g., two relative momenta p, q and the total onshell momentum P . From three momenta one can form six Lorentz invariants (with $P^2 = -m_B^2$, where m_B is the mass of the baryon), so the 64 dressing functions depend on six variables.

Despite this, the Faddeev equation can be solved without any approximations on the amplitudes, i.e., including all tensors and Lorentz invariants in the system [35, 36]. The resulting nucleon and Δ -baryon masses are shown in Fig. 8. Here the rainbow-ladder truncation (32) was employed, with the same Maris-Tandy interaction $\alpha(k^2)$ which depends on one relevant parameter Λ fixed by f_π . Interestingly, the resulting nucleon mass is 940 MeV — it appears that rainbow-ladder is a *very* good starting point towards understanding not only the properties of mesons but also those of baryons. Similar calculations have also been successfully employed for other octet and decuplet baryons as well as for heavy baryons [37–39].

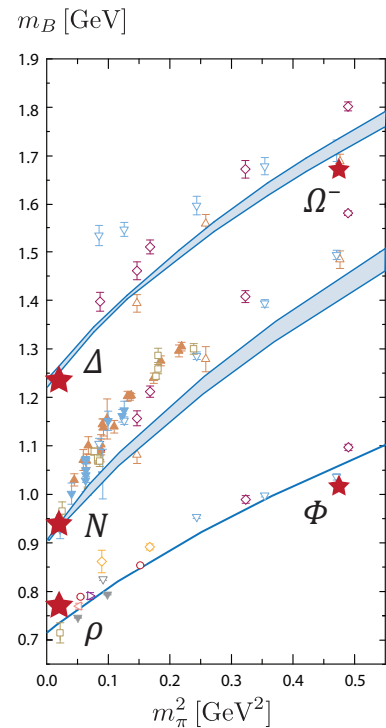


Fig. 8 Nucleon, Δ -baryon and ρ -meson masses as a function of the current-quark mass. The bands are the calculated masses and show the sensitivity to the shape parameter η . The stars are the experimental masses, and the points are lattice results for comparison [5].

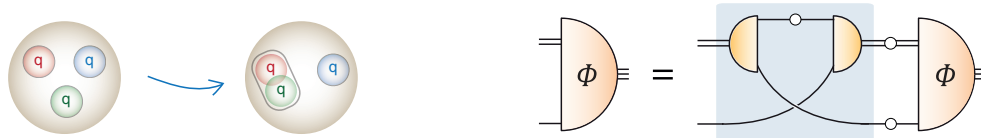


Fig. 9 Left: Two quarks inside a baryon can cluster to a diquark. Right: Quark-diquark BSE.

4.2 Diquarks

What is the internal structure of baryons? A longstanding idea is that two quarks inside a baryon may cluster to a colored diquark [40, 41]. From

$$\mathbf{3} \otimes \mathbf{3} \otimes \mathbf{3} = (\bar{\mathbf{3}} \oplus \mathbf{6}) \otimes \mathbf{3} = \mathbf{1} \oplus \mathbf{8} \oplus \mathbf{8} \oplus \mathbf{10} \quad (40)$$

one can see that quarks may form color-antitriplet ($\bar{\mathbf{3}}$) and color-sextet ($\mathbf{6}$) diquarks, but only a $\bar{\mathbf{3}}$ diquark can combine with the remaining quark to form a color-singlet baryon. From the color algebra one can also show that the quark-quark interaction in the $\bar{\mathbf{3}}$ channel is attractive and half as strong as that for color-singlet mesons.

Traditionally, one argument in favor of diquark correlations in baryons has been the so-called ‘missing-resonances problem’, which is the observation that nonrelativistic quark models predict too many states in the baryon excitation spectrum. A three-quark system has two excitation modes, a ‘ ρ oscillator’ between two quarks and a ‘ λ oscillator’ between those quarks and the remaining quark. If quarks formed pointlike diquarks, this would freeze the ρ mode and thus reduce the number of excitations. However, over the last decade new states have been found in photo- and electroproduction, which calls this simple idea into question [42]; moreover, static diquarks that cannot exchange their roles would also break the permutation symmetry. On the other hand, non-pointlike diquark correlations in the form of two-body clusters appear quite naturally in the three-body equation. With only a few assumptions [5], the Faddeev equation in Fig. 7 can be converted into a quark-diquark BSE which is shown in Fig. 9. Here the interaction proceeds through a ping-pong quark exchange between quark and diquark, so that the diquarks permanently exchange their roles. Furthermore, this two-body BSE can be solved using the very same ingredients as for the three-body equation, which allows for a direct comparison between the two approaches.

The top panel in Fig. 10 shows the resulting light-baryon excitation spectrum for $J = 1/2^\pm$ and $J = 3/2^\pm$ quantum numbers [43]. The open boxes are the three-quark results, the filled boxes the quark-diquark results, and the hatched boxes are the PDG masses. One can see that the three-quark and quark-diquark results in the nucleon $1/2^+$ and Δ -baryon $3/2^+$ channels are very similar. Apparently, diquark clustering is a good way to think about baryons!

For the remaining channels, we briefly need to discuss the diquark properties. The lightest ones are the scalar diquarks (with $J^P = 0^+$, isospin $I = 0$ and masses around 800 MeV), followed by the axialvector diquarks ($J^P = 1^+$, isospin $I = 1$ and masses around 1 GeV), then pseudoscalar diquarks, vector diquarks, etc. It turns out that the scalar (axialvector) diquarks are closely linked with the pseudoscalar (vector) mesons; their BSEs differ only by a color factor 2. In the literature these are also often called ‘good’ and ‘bad’ diquarks, although there is nothing good or bad about them: both scalar and axialvector diquarks contribute to the nucleon and Roper resonance, and for the Δ baryon only axialvector diquarks (the ‘bad’ ones!) can contribute due to isospin.

Quoting a famous spaghetti Western, if scalar diquarks are ‘good’ and axialvector diquarks ‘bad’, then the higher-lying pseudoscalar and vector diquarks are indeed ‘ugly’. These are the analogues of the more problematic scalar and axialvector mesons, whose rainbow-ladder masses come out too low. They also strongly affect the remaining baryon channels in Fig. 10, i.e., nucleon $1/2^-$ and $3/2^\pm$ and Δ -baryon $3/2^-$ and $1/2^\pm$, whose masses also come out too low. In the three-quark approach, where diquarks do not appear explicitly, there is nothing one can do about this except go beyond rainbow-ladder. However, in the quark-diquark system one can tune the properties of the ‘ugly’ diquarks: One can simulate beyond rainbow-ladder effects by introducing one additional strength parameter, which is fixed in the meson sector and pushes up the axialvector mesons to their experimental ballpark. This also pushes up the baryon masses in these channels, which leads to the plot in Fig. 10. It shows a 1:1 correspondence between the calculated and experimental spectrum, and there are no missing states. In total this gives two active parameters, the rainbow-ladder scale Λ (fixed by f_π) and the diquark strength parameter (fixed by the a_1/b_1 mesons). This may be compared to quark models, where sometimes a dozen parameters are needed to describe the spectrum!

Speaking of the quark model, in nonrelativistic quark models each baryon is usually identified with a definite orbital angular momentum L . The nucleon and Δ -baryon have $L = 0$, the $N(1535)$ and $N(1650)$ have $L = 1$, and so on. Relativistically this is no longer so, because only the total angular momentum J is a good quantum number while different L components mix. For example, each tensor $\tau_i(p, q, P)$ in Eq. (39) carries a specific value of L in the baryon’s rest frame, but the baryon is a superposition of all of them. This is shown in the bottom of Fig. 10: The nucleon and $\Delta(1232)$ carry $L = 0$ (s -wave) but also $L = 1$ (p -wave) components, where the latter are relativistic effects. In many cases the leading components agree with the quark model identification, so the nonrelativistic quark model clearly shines through in the spectrum. In general, however, relativity is quite important for the light baryon spectrum.

A quark-diquark picture is also appropriate for hyperons containing strange quarks, as well as for charmed baryons such as Σ_c and Λ_c which consist of two light quarks and one charm quark. Denoting up and down by n , it is often assumed that charmed baryons form ‘planetary’ systems made of a light (m) diquark that ‘orbits’ around the heavier charm quark. However, the Faddeev calculations do not support this picture [44, 45]. Rather, the $(nc)n$ configurations are dominant and contribute about 60% to the norm of the state, while the $(nm)c$ configurations contribute only 40%. Therefore, a charmed baryon actually spends most of its time in a $(nc)n$ configuration.

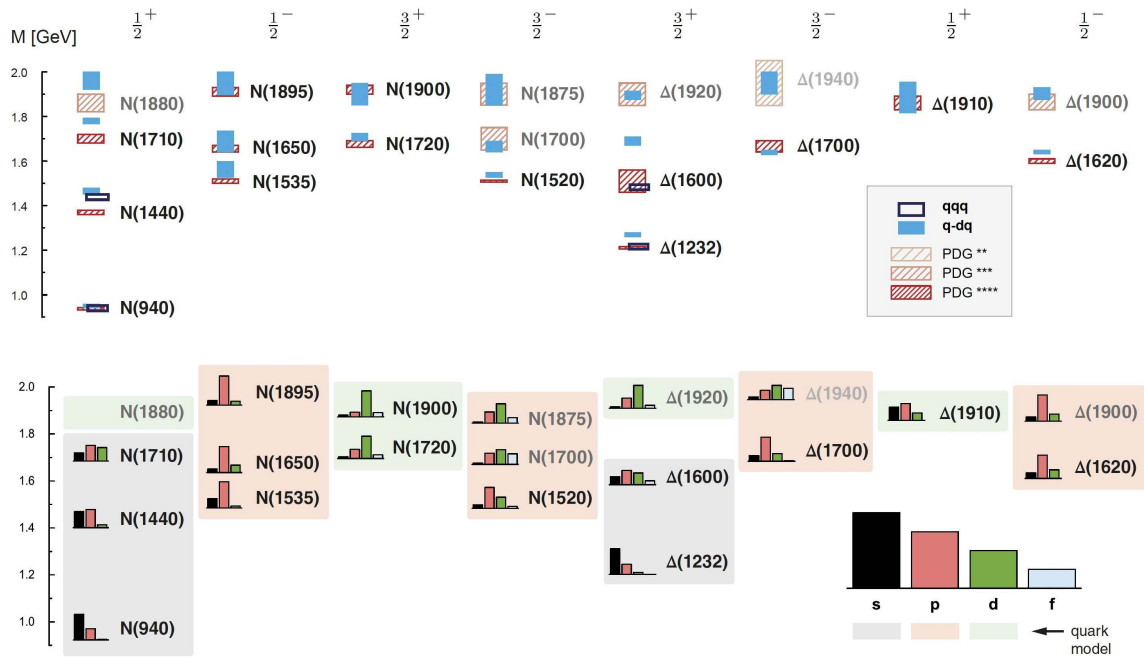


Fig. 10 Top: Light baryon spectrum from the three-quark and quark-diquark equations compared to the PDG [43]. The three-quark and quark-diquark in the nucleon $1/2^+$ and Δ -baryon $3/2^+$ channels show good agreement, and there is a 1:1 correspondence between the calculated and experimental spectrum. Bottom: Orbital angular momentum components for the different states. The colored rectangles correspond to the orbital angular momentum assignments in the nonrelativistic quark model.

5 Four-quark states

5.1 Dynamical generation of resonances

Given that diquarks appear to play an important role for baryons, it is natural to ask whether diquark clustering also extends to exotic hadrons. The oldest exotic meson candidate is the $\sigma/f_0(500)$ meson, which is part of the lightest scalar meson nonet with quantum numbers $J^{PC} = 0^{++}$ shown in Fig. 11. The σ has several unusual properties. Viewed as ordinary $q\bar{q}$ states, the a_0 and σ should be approximately mass-degenerate, like the ρ and ω mesons in the 1^{--} vector channel, since both are made of light up and down quarks. The kaon-like $\kappa/K_0^*(700)$ with one strange quark should be heavier, followed by the $f_0(980)$ which is the $s\bar{s}$ state. However, this is not what we see in Fig. 11: Instead, the a_0 and f_0 are mass-degenerate and the heaviest states, which does not make any sense. In the nonrelativistic quark model, the light scalar nonet also carries orbital angular momentum $L = 1$ and should thus be considerably heavier than the pseudoscalar and vector mesons. Furthermore, the σ has a huge decay width compared to other $q\bar{q}$ states, which makes it hard to see in experiments and has led to a long controversy regarding its status in the PDG [46].

A possible explanation is that these states could be four-quark states in the form of diquark-antidiquark clusters $(qq)(\bar{q}\bar{q})$ [47, 48]. According to Eq. (40), a scalar $\bar{\mathbf{3}}$ diquark can combine with a scalar $\mathbf{3}$ antidiquark to form a color singlet. This produces again a nonet of states, but now the mass ordering is reversed: The σ is the lightest state because it is made of four light quarks, while the κ contains one strange quark and the a_0 and f_0 two, which explains the mass ordering. It would also explain the large decay widths, since the σ can simply fall apart to produce two pions without exchanging gluons. Alternatively, the observation that the a_0 and f_0 sit very close to the $K\bar{K}$ threshold points toward a molecular picture $(q\bar{q})(q\bar{q})$ [49]. In any case, there seems to be a general consensus by now that the light scalar mesons are not $q\bar{q}$ but rather four-quark states [46].

To study the light scalar mesons with functional methods, one should solve the four-quark Bethe-Salpeter (or Faddeev-Yakubowski) equation shown in the left of Fig. 12. In this case, one has permutations of two-body irreducible kernels (minus subtraction terms to avoid overcounting) plus three- and four-body kernels. Keeping only the two-body kernels, the situation is worse compared to baryons because the wave function (the four-body analogue of Eqs. (24) and (39)) depends on four independent momenta p_1, \dots, p_4 . This results in hundreds of Dirac tensors, whose dressing functions f_i depend on nine kinematic variables (plus the total onshell momentum variable P^2). The resulting BSE is an eigenvalue equation whose kernel matrix has a dimension of about 10^{13} — this is impossible to solve even with the best computers that are available today.

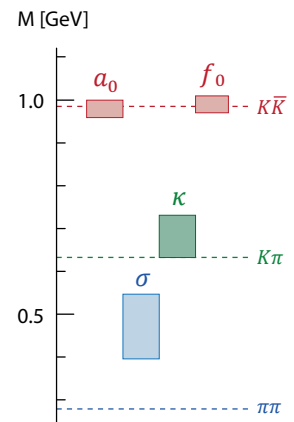


Fig. 11 Light scalar meson spectrum from the PDG [11].

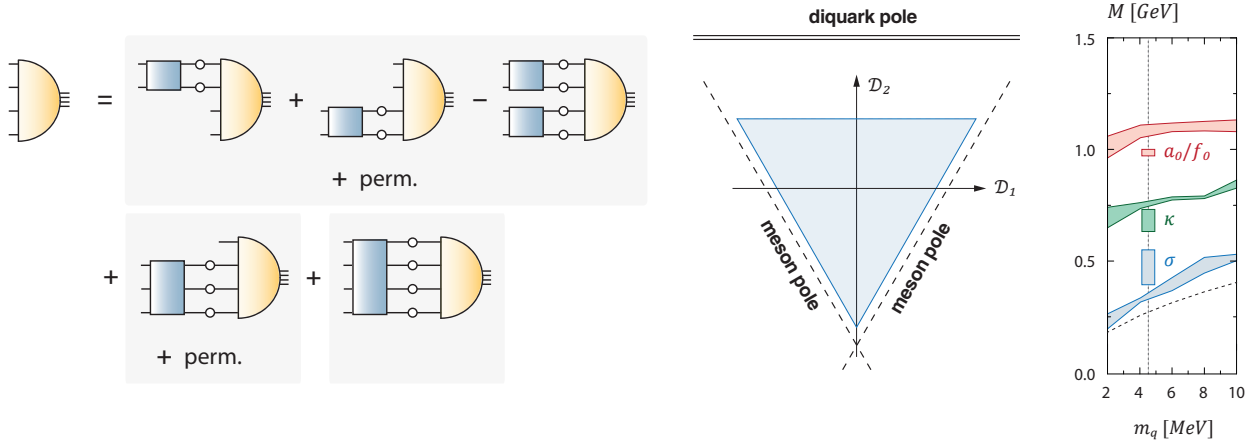


Fig. 12 Left: Four-quark Bethe-Salpeter equation with two-, three- and four-body kernels. Center: Mandelstam plane where the meson-meson and diquark-antidiquark poles become visible. The colored triangle is the integration region in the BSE. Right: Light scalar meson spectrum from the four-quark equation in the vicinity of the light current-quark mass [50]; the boxes are the PDG masses.

A very useful way to construct approximations is to group these variables in multiplets of the permutation group S_4 , because this allows one to switch off groups of variables without breaking the symmetries of the system. It turns out that one can arrange the $1 + 2 + 3 + 3 = 9$ variables into a singlet \mathcal{S}_0 , a doublet \mathcal{D} and two triplets. The most important variables are the singlet and doublet. The singlet is the symmetric variable $\mathcal{S}_0 \sim p_1^2 + p_2^2 + p_3^2 + p_4^2$ and carries the scale. The doublet forms the Mandelstam plane in the center panel of Fig. 12, which shows the internal two-body poles. If we label the quarks in the $qq\bar{q}\bar{q}$ wave function by 1, 2 and the antiquarks by 3, 4, then the system can form internal diquark-antidiquark clusters, (12)(34), and two meson-meson clusters, (13)(24) and (14)(23). These are dynamically generated in the four-quark BSE and show up as poles in the Mandelstam plane. Because the pions are much lighter than the diquarks, the pion poles are much closer to the integration region (the colored triangle) than the diquark poles. Thus, the four-body system is dominated by the pions: If the four-body BSE is solved keeping the variable \mathcal{S}_0 only, the resulting σ mass is about 1500 MeV; the two triplets only have subleading effects; but if the doublet \mathcal{D} is included, the mass jumps down to ~ 350 MeV [50]. The resulting mass pattern for the light scalar mesons qualitatively agrees with the experimental spectrum, as shown in the right panel of Fig. 12 in the vicinity of the light current-quark mass.

What happened here is quite interesting: One starts out with four quarks which interact by gluons. However, in the solution process the four-quark wave function dynamically generates pion poles, which produce a resonance mechanism. Thus, the resulting σ meson is at the same time a four-quark state *and* a $\pi\pi$ resonance! This also explains why it is so light, since the dominant internal clusters are not the diquarks but rather the pions, the pseudoscalar Goldstone bosons in QCD. So, even though the underlying mechanism — the dynamical generation of two-body clusters — is similar as for baryons, the physical consequences are very different.

This mechanism also builds a bridge to effective field theories, where two-body BSEs and scattering equations are solved using hadronic degrees of freedom [51]. To make an analogy with civil engineering, suppose the hadronic degrees of freedom from the effective Lagrangian live on the first floor. Solving hadronic BSEs, these dynamically create resonances on the second floor. In the four-quark equation, we take the elevator and go a level deeper: The fundamental degrees of freedom are the quarks and gluons in the basement. Even though they are not directly observable, they keep the building running: They dynamically create hadrons on the first floor, which may dynamically create further resonances on the second floor. In the four-quark equation all this happens automatically without making assumptions (apart from practical approximations to make the numerical solutions feasible).

The remaining question concerns the $q\bar{q}$ contributions to the σ . Even though the σ resides on the second floor, it also has an office on the first floor since it may be a superposition of $qq\bar{q}\bar{q}$ and $q\bar{q}$ components. This can be studied by coupling the four-quark BSE with the $q\bar{q}$ BSE, from where one finds that the $q\bar{q}$ contributions are indeed rather small [16].

5.2 Heavy exotics

Compared to light mesons, where relativity and chiral symmetry are important, the heavy-quark sector is a much cleaner environment for studying exotics. Here the success of the non-relativistic quark model provides a basic measure for distinguishing ‘ordinary’ from ‘exotic’ mesons, namely through the deviation from the quark-model expectations. An abundance of new data in the charm and bottom region has established the existence of four-quark states [51, 54–60]. Many of them are close to meson-meson thresholds, which points towards a molecular nature. In the following we consider two types of exotic mesons:

- *Hidden-flavor states* of the type $Q\bar{Q}q\bar{q}$, where $Q = c, b$ is a heavy quark and $q = u, d, s$. If these states carry isospin $I = 0$, they can still mix with ordinary $Q\bar{Q}$ mesons. The most prominent example is the $\chi_{c1}(3872)$ with quantum numbers $I(J^{PC}) = 0(1^{++})$, which was first reported by Belle in 2003 [61]. It has several properties that do not fit into a conventional charmonium picture, like its mass which is indistinguishable from the $D^0\bar{D}^{*0}$ threshold, its narrow width (< 1.2 MeV) which is much smaller than potential-model predictions

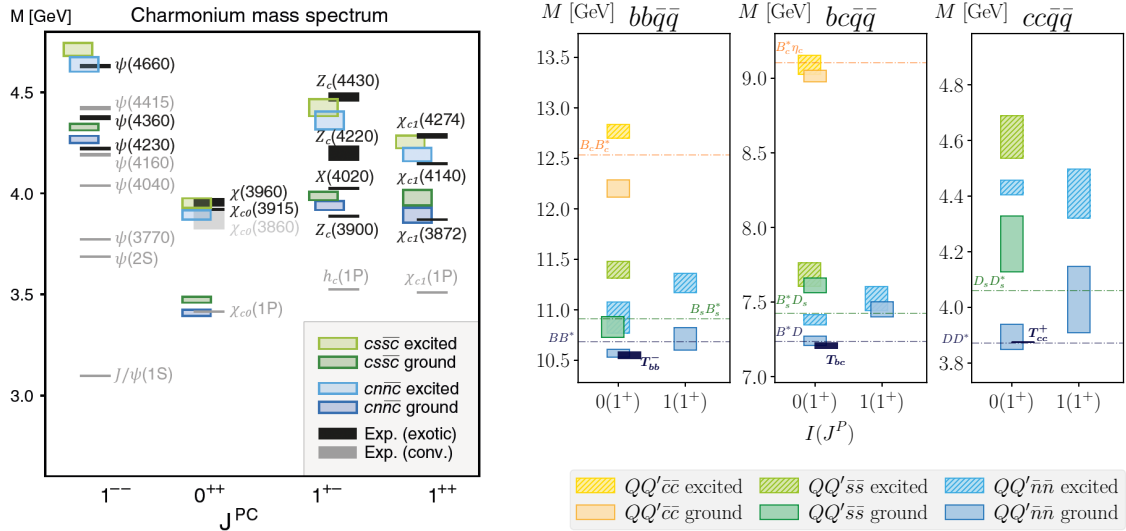


Fig. 13 Left: Hidden-charm spectrum. The gray boxes are the conventional $c\bar{c}$ states from the PDG, and the black boxes are the exotic states. The colored boxes are the results from the four-quark equation [52]. Right: Open-flavor spectrum for $J^P = 1^+$ and quark content $bb\bar{q}\bar{q}$, $bc\bar{q}\bar{q}$ and $cc\bar{q}\bar{q}$. The levels in black are the experimental T_{cc}^+ mass and the theory predictions for its partners. The colored boxes are the four-quark results [53].

for the first excited $c\bar{c}$ state, and its unusual decay modes. For other exotic candidates like the $\psi(4230)$ in the 1^{--} vector channel, their exotic assignment is mainly due to the overpopulation of the 1^{--} channel with regard to well-established $c\bar{c}$ states. The $Z_c(3900)$ and $Z_c(4430)$ with $J^{PC} = 1^{+-}$, on the other hand, carry charge and are thus manifestly exotic since their minimal quark content is $c\bar{c}u\bar{d}$.

- *Open-flavor states* of the type $QQ\bar{q}\bar{q}$, which are manifestly exotic and cannot be made of $q\bar{q}$. So far, only one state has been found experimentally, the $T_{cc}(3875)^+$ with quark content $cc\bar{u}\bar{d}$, which is extremely close to the D^0D^{*+} threshold [62]. If the masses of the heavy quarks are sufficiently large and those of the light quarks sufficiently small, such states are expected to form deeply bound states [63, 64], like the T_{bb}^- made of $bb\bar{u}\bar{d}$ which is predicted by many theoretical calculations.

Meanwhile also states with one heavy quark ($Q\bar{q}\bar{q}\bar{q}$) and four heavy quarks ($QQ\bar{Q}\bar{Q}$) have been found with LHCb, so the list of heavy exotics keeps ever growing [34].

What can the four-quark equation say about heavy exotics? In principle, the approach discussed in Sec. 5.1 can be taken over without modifications. For hidden-charm states, the three sides of the triangle in Fig. 12 correspond to the three possible two-body clusters in the system: diquark-antidiquark ($Qq)(\bar{Q}\bar{q})$, meson molecule ($Q\bar{q})(q\bar{Q})$, or hadroquarkonium ($Q\bar{Q})(q\bar{q})$. Take for example the $\chi_{c1}(3872)$ made of $c\bar{c}n\bar{n}$, where $n = u, d$ are the light up and down quarks. Here the lightest clusters are a meson-molecule configuration $(c\bar{n})(n\bar{c})$ which is $D\bar{D}^*$, a hadroquarkonium component $(c\bar{c})(n\bar{n})$ which is $J/\psi\omega$, and a diquark-antidiquark $(cn)(\bar{c}\bar{n})$ configuration which is substantially heavier.

The resulting spectrum is shown in the left panel of Fig. 13. The gray levels are the conventional $c\bar{c}$ states from experiment, the black levels the exotic candidates, and the colored boxes are the BSE results for $cn\bar{n}\bar{c}$ and $cs\bar{s}\bar{c}$ states (ground state and first excited state each). In general, the proximity of the $cn\bar{n}\bar{c}$ and $cs\bar{s}\bar{c}$ states leads to a densely populated spectrum. One can see that the $\chi_{c1}(3872)$ in the 1^{++} channel is nicely reproduced (note, however, that the backcoupling of the $c\bar{c}$ components is not yet included here). For the 1^{--} and 1^{+-} states an identification is also possible. An exception is the 0^{++} channel, where the four-body results are close to the ordinary $c\bar{c}$ state. Concerning the internal structure of these states, the 1^{--} , 0^{++} and 1^{+-} channels are strongly dominated by meson-molecule configurations (like $D\bar{D}^*$ for the $\chi_{c1}(3872)$), while in the 1^{++} channel they are mixture of meson-molecule and hadrocharmonium components, where the latter is dominant. The diquark components are almost negligible in all cases.

For open-charm states the situation is quite different. Here the two-body clusters are diquark-antidiquark ($QQ)(\bar{q}\bar{q})$ and two degenerate meson-meson configurations ($Q\bar{q})(Q\bar{q})$. The resulting spectra for $bb\bar{q}\bar{q}$, $bc\bar{q}\bar{q}$ and $cc\bar{q}\bar{q}$ states with $J^P = 1^+$ are shown in the right panels of Fig. 13. In the rightmost plot, the black level is the experimental mass of the T_{cc}^+ , while its partners in the other two plots are theory predictions. Also here, the BSE results nicely match the ground states. The internal structure, however, turns out to be very different. The T_{cc}^+ is almost entirely dominated by the molecular DD^* component due to its proximity to the threshold. Its bottom partner T_{bb}^- , on the other hand, is a mixture of everything with a dominant diquark-antidiquark component.

One can see that the strength of the four-body equation is its ability to *predict* the dominant two-body clusters. This is different from model calculations, where one settles on one specific component (diquark-antidiquark, meson molecule, hadroquarkonium) from the start and makes predictions for that component. However, the size of these components may be very different on a case-by-case basis or even a complicated mixture, and it is a dynamical question which component is the leading one. In the four-body BSE these components are dynamically generated from the quarks and gluons in the equation without prior assumptions.

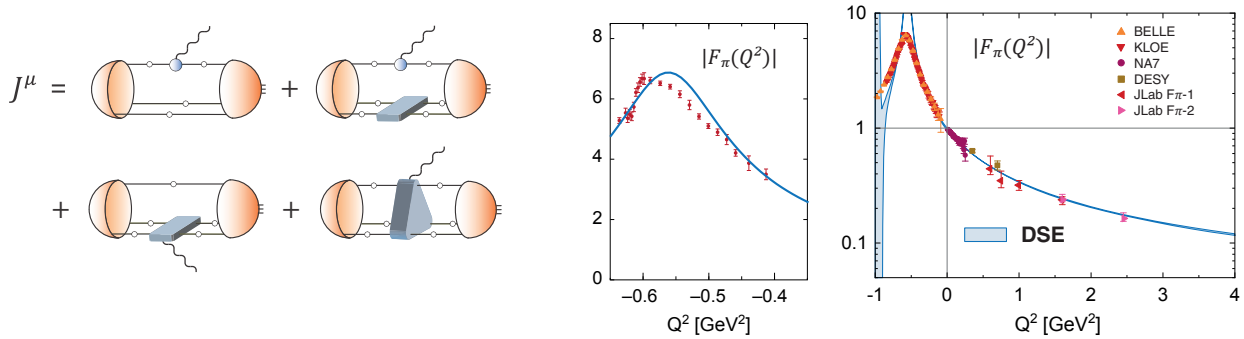


Fig. 14 Left: Current matrix element for a three-quark system. The photon couples to the quarks and to the two- and three-quark irreducible kernels. Center and right: Electromagnetic pion form factor in the spacelike and timelike region, with DSE/BSE results compared to experimental data. The right panel shows the rainbow-ladder result, where the timelike ρ -meson pole is visible [65]. The center panel is the result of a calculation beyond rainbow-ladder including the $\pi\pi$ channel; here the pole is shifted onto the second Riemann sheet and only the bump is visible on the real axis [66].

6 Hadron structure

So far we have talked about hadron *spectroscopy* with functional methods. To recapitulate, the strategy is to solve two-, three- and four-body BSEs (Figs. 4, 7, 9 and 12), whose ingredients are QCD's n -point functions which must be calculated beforehand. The outcomes of the BSEs are the masses, i.e., the excitation spectra for the various $J^{P(C)}$ channels, and the hadron wave functions, i.e., their Bethe-Salpeter amplitudes. With the wave functions at hand, one can go further and calculate hadron *structure* properties such as form factors, parton distributions and scattering amplitudes, which are encoded in the hadron matrix elements.

These matrix elements can be derived in analogy to the derivation of the BSE itself in Sec. 3.1. For example, to obtain an electromagnetic nucleon-to-resonance transition matrix element ($\gamma^* N \rightarrow N^*$), one starts from the quark six-point function (the three-quark analogue of the $q\bar{q}$ four-point function in Fig. 5), couples a photon to it, and inserts a complete set of states to the left and right of the current insertion. This produces all possible baryon poles, once on the left and once on the right of the photon insertion. The matrix element is then the residue at the (N, N^*) double pole [67]. Once again, it does not matter if the poles are real or complex, i.e. whether one deals with bound states or resonances, because the current matrix element is simply the residue at the pole. The result is shown in the left panel of Fig. 14: The photon couples to the quarks and to the two- and three-body irreducible kernels. Note that this is an exact expression in QFT. In a rainbow-ladder truncation only the first two diagrams survive, because the photon cannot couple to a gluon and the three-body kernel is omitted.

The only new ingredient is then the quark-photon vertex, which is the $q\bar{q}$ four-point function \mathbf{G} in Fig. 5 with one $q\bar{q}$ pair contracted to form a photon. The scattering equation for \mathbf{G} then immediately yields an inhomogeneous BSE for the vertex, which can be solved with the same input as outlined earlier and without further approximations [68]. The BSE for the quark-photon vertex has some interesting features. Because \mathbf{G} contains all possible meson poles, the quark-photon vertex must pick up all meson poles with the same quantum numbers of the photon. These are the vector mesons with $J^P = 1^-$. Thus, when solving the vertex BSE, these poles are dynamically generated in the solution. This is the underlying origin of vector-meson dominance, which dictates the shape of a spacelike electromagnetic form factor at low Q^2 : On the timelike side, the electromagnetic form factors of hadrons must have vector-meson poles.

As an example, the right panel in Fig. 14 shows the pion electromagnetic form factor, which has a pole at $Q^2 = -m_\rho^2$. This is an automatic feature when calculating the form factor and its ingredients systematically from their DSEs and BSEs. The normalization $F_\pi(0) = 1$ is also automatic as long as the BSE kernel satisfies the vector Ward-Takahashi identity. In reality these poles are bumps, because the ρ -meson is a resonance with a pole on the second Riemann sheet. The rainbow-ladder truncation generates a pole on the real axis corresponding to a bound state, but if one includes intermediate $\pi\pi$ channels in the BSE kernel, the ρ pole moves into the complex plane on the second Riemann sheet and the ρ meson becomes a resonance, as shown in the center panel.

Based on this, many form factor calculations have been done over the last decades, see e.g. [5, 41, 69] and references therein: meson electromagnetic and transition form factors, baryon elastic and transition form factors, axial and gravitational form factors, meson two-photon transition form factors that enter in the muon $g - 2$ problem, and so on. For baryons one finds similar conclusions as discussed in Sec. 4: The three-quark and quark-diquark results are very similar, and discrepancies between the two approaches are rather small. Discrepancies with experimental results mainly appear at small Q^2 , where meson-cloud effects become important. These are not yet captured by a rainbow-ladder truncation but, as we just mentioned, work in this direction is underway. Also a range of hadron structure calculations are available, e.g., for pion and kaon parton distribution functions [70], and scattering amplitudes such as $\pi\pi \rightarrow \pi\pi$, $\pi\gamma^* \rightarrow \pi\pi$ and $N\gamma^* \rightarrow N\gamma^*$ have been investigated as well [5, 71, 72].

7 Conclusions and outlook

We have seen that functional methods provide a systematic way to calculate hadron properties from quarks and gluons, the fundamental degrees of freedom of QCD. Despite 25+ years of work, the approach is still at a comparatively early stage given that the most hadron physics applications so far have employed the rainbow-ladder truncation, or minimal extensions of it, or simpler models. To systematically go beyond the status quo towards precision calculations, one needs to calculate QCD's n -point functions beyond the quark propagator which go into the BSE kernel: the gluon propagator, quark-gluon vertex, three- and four-gluon vertex, and so on. There are ongoing efforts in these directions using the Dyson-Schwinger equations [23–25, 73] shown in Fig. 1, the functional renormalization group [10, 74], and gauge-fixed lattice QCD [75–78]. A nice example is the glueball spectrum in Yang-Mills theory, i.e., QCD without quarks: Once the underlying n -point functions are calculated from their DSEs, the resulting glueball spectrum agrees with lattice QCD [79]. In the next years we will probably see similar advances along these lines towards QCD with dynamical quarks.

A parallel avenue is to expand the pool of observables that can be calculated with functional methods. As we have seen, applications for meson and baryon spectroscopy (including four-quark states) are reasonably advanced by now. The same can be said about form factors and parton distributions, as well as for applications towards finite temperature and density [7]. The next frontier are exotic quantum numbers, many-quark states, scattering amplitudes and weak interactions of hadrons, generalized parton distributions and transverse momentum distributions, or fragmentation functions and hadronization. Exploratory studies in several of these directions are already underway, and as the functional methods community is growing bigger we may see many more results in the future.

Acknowledgments

This work was supported by the Austrian Science Fund FWF under grant number 10.55776/PAT2089624 and by the Portuguese Science fund FCT under grant number CERN/FIS-PAR/0023/2021. This work contributes to the aims of the USDOE ExoHad Topical Collaboration, contract DE-SC0023598.

References

- [1] C. Gattringer, C. B. Lang, Quantum chromodynamics on the lattice, vol. 788, Springer, Berlin 2010, ISBN 978-3-642-01849-7, 978-3-642-01850-3, doi:10.1007/978-3-642-01850-3.
- [2] C. D. Roberts, A. G. Williams, Dyson-Schwinger equations and their application to hadronic physics, Prog. Part. Nucl. Phys. 33 (1994) 477–575, doi:10.1016/0146-6410(94)90049-3, [hep-ph/9403224](#).
- [3] R. Alkofer, L. von Smekal, The Infrared behavior of QCD Green's functions: Confinement dynamical symmetry breaking, and hadrons as relativistic bound states, Phys. Rept. 353 (2001) 281, doi:10.1016/S0370-1573(01)00010-2, [hep-ph/0007355](#).
- [4] A. Bashir, L. Chang, I. C. Cloet, B. El-Bennich, Y.-X. Liu, C. D. Roberts, P. C. Tandy, Collective perspective on advances in Dyson-Schwinger Equation QCD, Commun. Theor. Phys. 58 (2012) 79–134, doi:10.1088/0253-6102/58/1/16, [1201.3366](#).
- [5] G. Eichmann, H. Sanchis-Alepuz, R. Williams, R. Alkofer, C. S. Fischer, Baryons as relativistic three-quark bound states, Prog. Part. Nucl. Phys. 91 (2016) 1–100, doi:10.1016/j.ppnp.2016.07.001, [1606.09602](#).
- [6] M. Q. Huber, Nonperturbative properties of Yang–Mills theories, Phys. Rept. 879 (2020) 1–92, doi:10.1016/j.physrep.2020.04.004, [1808.05227](#).
- [7] C. S. Fischer, QCD at finite temperature and chemical potential from Dyson–Schwinger equations, Prog. Part. Nucl. Phys. 105 (2019) 1–60, doi:10.1016/j.ppnp.2019.01.002, [1810.12938](#).
- [8] J. Berges, N. Tetradis, C. Wetterich, Nonperturbative renormalization flow in quantum field theory and statistical physics, Phys. Rept. 363 (2002) 223–386, doi:10.1016/S0370-1573(01)00098-9, [hep-ph/0005122](#).
- [9] J. M. Pawłowski, Aspects of the functional renormalisation group, Annals Phys. 322 (2007) 2831–2915, doi:10.1016/j.aop.2007.01.007, [hep-th/0512261](#).
- [10] N. Dupuis, L. Canet, A. Eichhorn, W. Metzner, J. M. Pawłowski, M. Tissier, N. Wschebor, The nonperturbative functional renormalization group and its applications, Phys. Rept. 910 (2021) 1–114, doi:10.1016/j.physrep.2021.01.001, [2006.04853](#).
- [11] G. Eichmann, C. S. Fischer, W. Heupel, N. Santowsky, P. C. Wallbott, Four-Quark States from Functional Methods, Few Body Syst. 61 (4) (2020) 38, doi:10.1007/s00601-020-01571-3, [2008.10240](#).
- [12] C. D. Roberts, M. S. Bhagwat, A. Holl, S. V. Wright, Aspects of hadron physics, Eur. Phys. J. ST 140 (2007) 53–116, doi:10.1140/epjst/e2007-00003-5, [0802.0217](#).
- [13] H. J. Munczek, A. M. Nemirovsky, The Ground State q anti- q Mass Spectrum in QCD, Phys. Rev. D 28 (1983) 181, doi:10.1103/PhysRevD.28.181.
- [14] P. Maris, C. D. Roberts, P. C. Tandy, Pion mass and decay constant, Phys. Lett. B 420 (1998) 267–273, doi:10.1016/S0370-2693(97)01535-9, [nucl-th/9707003](#).
- [15] Steven Weinberg, The Quantum theory of fields. Vol. 1: Foundations, Cambridge University Press 2005, ISBN 978-0-521-67053-1, 978-0-511-25204-4, doi:10.1017/CBO9781139644167.
- [16] N. Santowsky, G. Eichmann, Christian S. Fischer, P. C. Wallbott, R. Williams, σ -meson: Four-quark versus two-quark components and decay width in a Bethe-Salpeter approach, Phys. Rev. D 102 (5) (2020) 056014, doi:10.1103/PhysRevD.102.056014, [2007.06495](#).
- [17] Gernot Eichmann, More about the light baryon spectrum, Few Body Syst. 58 (2) (2017) 81, doi:10.1007/s00601-016-1200-3, [1611.10118](#).
- [18] P. Maris, P. C. Tandy, Bethe-Salpeter study of vector meson masses and decay constants, Phys. Rev. C 60 (1999) 055214, doi:10.1103/PhysRevC.60.055214, [nucl-th/9905056](#).
- [19] S.-X. Qin, L. Chang, Y.-X. Liu, C. D. Roberts, D. J. Wilson, Interaction model for the gap equation, Phys. Rev. C 84 (2011) 042202, doi:10.1103/PhysRevC.84.042202, [1108.0603](#).
- [20] P. Maris, P. C. Tandy, QCD modeling of hadron physics, Nucl. Phys. B Proc. Suppl. 161 (2006) 136–152, doi:10.1016/j.nuclphysbps.2006.08.012, [nucl-th/0511017](#).

- [21] F. Gao, A. S. Miramontes, J. Papavassiliou, J. M. Pawłowski, Heavy-light mesons from a flavour-dependent interaction (2024), [2411.19680](#).
- [22] L. Chang, C. D. Roberts, Sketching the Bethe-Salpeter kernel, *Phys. Rev. Lett.* 103 (2009) 081601, doi:10.1103/PhysRevLett.103.081601, [0903.5461](#).
- [23] M. Q. Huber, Correlation functions of Landau gauge Yang-Mills theory, *Phys. Rev. D* 101 (2020) 114009, doi:10.1103/PhysRevD.101.114009, [2003.13703](#).
- [24] G. Eichmann, J. M. Pawłowski, J. M. Silva, Mass generation in Landau-gauge Yang-Mills theory, *Phys. Rev. D* 104 (11) (2021) 114016, doi:10.1103/PhysRevD.104.114016, [2107.05352](#).
- [25] M. N. Ferreira, J. Papavassiliou, Gauge Sector Dynamics in QCD, *Particles* 6 (1) (2023) 312–363, doi:10.3390/particles6010017, [2301.02314](#).
- [26] H. Pagels, S. Stokar, The Pion Decay Constant, Electromagnetic Form-Factor and Quark Electromagnetic Selfenergy in QCD, *Phys. Rev. D* 20 (1979) 2947, doi:10.1103/PhysRevD.20.2947.
- [27] E. Klempt, J.-M. Richard, Baryon spectroscopy, *Rev. Mod. Phys.* 82 (2010) 1095–1153, doi:10.1103/RevModPhys.82.1095, [0901.2055](#).
- [28] L. Tiator, D. Drechsel, S. S. Kamalov, M. Vanderhaeghen, Electromagnetic Excitation of Nucleon Resonances, *Eur. Phys. J. ST* 198 (2011) 141–170, doi:10.1140/epjst/e2011-01488-9, [1109.6745](#).
- [29] I. G. Aznauryan, V. D. Burkert, Electroexcitation of nucleon resonances, *Prog. Part. Nucl. Phys.* 67 (2012) 1–54, doi:10.1016/j.pnpnp.2011.08.001, [1109.1720](#).
- [30] V. Crede, W. Roberts, Progress towards understanding baryon resonances, *Rept. Prog. Phys.* 76 (2013) 076301, doi:10.1088/0034-4885/76/7/076301, [1302.7299](#).
- [31] F. Gross, et al., 50 Years of Quantum Chromodynamics, *Eur. Phys. J. C* 83 (2023) 1125, doi:10.1140/epjc/s10052-023-11949-2, [2212.11107](#).
- [32] A. Thiel, F. Afzal, Y. Wunderlich, Light Baryon Spectroscopy, *Prog. Part. Nucl. Phys.* 125 (2022) 103949, doi:10.1016/j.pnpnp.2022.103949, [2202.05055](#).
- [33] M. Mai, Review of the $\Lambda(1405)$ A curious case of a strangeness resonance, *Eur. Phys. J. ST* 230 (6) (2021) 1593–1607, doi:10.1140/epjs/s11734-021-00144-7, [2010.00056](#).
- [34] P. Koppenburg (LHCb collaboration), List of hadrons observed at the LHC, [LHCb-FIGURE-2021-001](#) 2021, see [2025 update online](#), URL <https://cds.cern.ch/record/2693187>.
- [35] G. Eichmann, R. Alkofer, A. Krassnigg, D. Nicmorus, Nucleon mass from a covariant three-quark Faddeev equation, *Phys. Rev. Lett.* 104 (2010) 201601, doi:10.1103/PhysRevLett.104.201601, [0912.2246](#).
- [36] G. Eichmann, Nucleon electromagnetic form factors from the covariant Faddeev equation, *Phys. Rev. D* 84 (2011) 014014, doi:10.1103/PhysRevD.84.014014, [1104.4505](#).
- [37] H. Sanchis-Alepuz, C. S. Fischer, Octet and Decuplet masses: a covariant three-body Faddeev calculation, *Phys. Rev. D* 90 (9) (2014) 096001, doi:10.1103/PhysRevD.90.096001, [1408.5577](#).
- [38] S.-X. Qin, C. D. Roberts, S. M. Schmidt, Poincaré-covariant analysis of heavy-quark baryons, *Phys. Rev. D* 97 (11) (2018) 114017, doi:10.1103/PhysRevD.97.114017, [1801.09697](#).
- [39] S.-X. Qin, C. D. Roberts, S. M. Schmidt, Spectrum of light- and heavy-baryons, *Few Body Syst.* 60 (2) (2019) 26, doi:10.1007/s00601-019-1488-x, [1902.00026](#).
- [40] M. Anselmino, E. Predazzi, S. Ekelin, S. Fredriksson, D. B. Lichtenberg, Diquarks, *Rev. Mod. Phys.* 65 (1993) 1199–1234, doi:10.1103/RevModPhys.65.1199.
- [41] M. Yu. Barabanov, et al., Diquark correlations in hadron physics: Origin, impact and evidence, *Prog. Part. Nucl. Phys.* 116 (2021) 103835, doi:10.1016/j.pnpnp.2020.103835, [2008.07630](#).
- [42] V. A. Nikonov, A. V. Anisovich, E. Klempt, A. V. Sarantsev, U. Thoma, Further evidence for $N(1900)P(13)$ from photoproduction of hyperons, *Phys. Lett. B* 662 (2008) 245–251, doi:10.1016/j.physletb.2008.03.004, [0707.3600](#).
- [43] G. Eichmann, C. S. Fischer, H. Sanchis-Alepuz, Light baryons and their excitations, *Phys. Rev. D* 94 (9) (2016) 094033, doi:10.1103/PhysRevD.94.094033, [1607.05748](#).
- [44] P.-L. Yin, C. Chen, G. Krein, C. D. Roberts, J. Segovia, S.-S. Xu, Masses of ground-state mesons and baryons, including those with heavy quarks, *Phys. Rev. D* 100 (3) (2019) 034008, doi:10.1103/PhysRevD.100.034008, [1903.00160](#).
- [45] A. Torcato, A. Arriaga, G. Eichmann, M. T. Peña, Heavy Baryon Spectroscopy in a Quark–Diquark Approach, *Few Body Syst.* 64 (3) (2023) 45, doi:10.1007/s00601-023-01826-9, [2304.07393](#).
- [46] J. R. Pelaez, From controversy to precision on the sigma meson: a review on the status of the non-ordinary $f_0(500)$ resonance, *Phys. Rept.* 658 (2016) 1, doi:10.1016/j.physrep.2016.09.001, [1510.00653](#).
- [47] R. L. Jaffe, Multi-Quark Hadrons. 1. The Phenomenology of (2 Quark 2 anti-Quark) Mesons, *Phys. Rev. D* 15 (1977) 267, doi:10.1103/PhysRevD.15.267.
- [48] G. 't Hooft, G. Isidori, L. Maiani, A. D. Polosa, V. Riquer, A Theory of Scalar Mesons, *Phys. Lett. B* 662 (2008) 424–430, doi:10.1016/j.physletb.2008.03.036, [0801.2288](#).
- [49] J. D. Weinstein, N. Isgur, K anti-K Molecules, *Phys. Rev. D* 41 (1990) 2236, doi:10.1103/PhysRevD.41.2236.
- [50] G. Eichmann, C. S. Fischer, W. Heupel, The light scalar mesons as tetraquarks, *Phys. Lett. B* 753 (2016) 282–287, doi:10.1016/j.physletb.2015.12.036, [1508.07178](#).
- [51] F.-K. Guo, C. Hanhart, U.-G. Meißner, Q. Wang, Q. Zhao, B.-S. Zou, Hadronic molecules, *Rev. Mod. Phys.* 90 (1) (2018) 015004, doi:10.1103/RevModPhys.90.015004, [Erratum: *Rev. Mod. Phys.* 94, 029901 (2022)], [1705.00141](#).
- [52] Joshua Hoffer, Gernot Eichmann, Christian S. Fischer, Hidden-flavor four-quark states in the charm and bottom region, *Phys. Rev. D* 109 (7) (2024) 074025, doi:10.1103/PhysRevD.109.074025, [2402.12830](#).
- [53] Joshua Hoffer, Gernot Eichmann, Christian S. Fischer, The structure of open-flavour four-quark states in the charm and bottom region (2024), [2409.05779](#).
- [54] Hua-Xing Chen, Wei Chen, Xiang Liu, Shi-Lin Zhu, The hidden-charm pentaquark and tetraquark states, *Phys. Rept.* 639 (2016) 1–121, doi:10.1016/j.physrep.2016.05.004, [1601.02092](#).
- [55] Richard F. Lebed, Ryan E. Mitchell, Eric S. Swanson, Heavy-Quark QCD Exotica, *Prog. Part. Nucl. Phys.* 93 (2017) 143–194, doi:10.1016/j.pnpnp.2016.11.003, [1610.04528](#).
- [56] A. Esposito, A. Pilloni, A. D. Polosa, Multiquark Resonances, *Phys. Rept.* 668 (2017) 1–97, doi:10.1016/j.physrep.2016.11.002, [1611.07920](#).
- [57] Ahmed Ali, Jens Sören Lange, Sheldon Stone, Exotics: Heavy Pentaquarks and Tetraquarks, *Prog. Part. Nucl. Phys.* 97 (2017) 123–198, doi:10.1016/j.pnpnp.2017.08.003, [1706.00610](#).
- [58] Stephen Lars Olsen, Tomasz Skwarnicki, Daria Ziemińska, Nonstandard heavy mesons and baryons: Experimental evidence, *Rev. Mod. Phys.* 90 (1) (2018) 015003, doi:10.1103/RevModPhys.90.015003, [1708.04012](#).
- [59] Yan-Rui Liu, Hua-Xing Chen, Wei Chen, Xiang Liu, Shi-Lin Zhu, Pentaquark and Tetraquark states, *Prog. Part. Nucl. Phys.* 107 (2019) 237–320, doi:10.1016/j.pnpnp.2019.04.003, [1903.11976](#).

- [60] Nora Brambilla, Simon Eidelman, Christoph Hanhart, Alexey Nefediev, Cheng-Ping Shen, Christopher E. Thomas, Antonio Vairo, Chang-Zheng Yuan, The XYZ states: experimental and theoretical status and perspectives, Phys. Rept. 873 (2020) 1–154, doi:10.1016/j.physrep.2020.05.001, [1907.07583](#).
- [61] S. K. Choi, et al. (Belle), Observation of a narrow charmonium-like state in exclusive $B^{\pm} \rightarrow K^{\pm} \pi^+ \pi^- J/\psi$ decays, Phys. Rev. Lett. 91 (2003) 262001, doi:10.1103/PhysRevLett.91.262001, [hep-ex/0309032](#).
- [62] Roel Aaij, et al. (LHCb), Observation of an exotic narrow doubly charmed tetraquark, Nature Phys. 18 (7) (2022) 751–754, doi:10.1038/s41567-022-01614-y, [2109.01038](#).
- [63] Anthony Francis, Renwick J. Hudspith, Randy Lewis, Kim Maltman, Lattice Prediction for Deeply Bound Doubly Heavy Tetraquarks, Phys. Rev. Lett. 118 (14) (2017) 142001, doi:10.1103/PhysRevLett.118.142001, [1607.05214](#).
- [64] Estia J. Eichten, Chris Quigg, Heavy-quark symmetry implies stable heavy tetraquark mesons $Q_i Q_j \bar{q}_k \bar{q}_l$, Phys. Rev. Lett. 119 (20) (2017) 202002, doi:10.1103/PhysRevLett.119.202002, [1707.09575](#).
- [65] Gernot Eichmann, Christian S. Fischer, Esther Weil, Richard Williams, Single pseudoscalar meson pole and pion box contributions to the anomalous magnetic moment of the muon, Phys. Lett. B 797 (2019) 134855, doi:10.1016/j.physletb.2019.134855, [Erratum: Phys.Lett.B 799, 135029 (2019)], [1903.10844](#).
- [66] Ángel S. Miramontes, Hèlios Sanchis Alepuz, Reinhard Alkofer, Elucidating the effect of intermediate resonances in the quark interaction kernel on the timelike electromagnetic pion form factor, Phys. Rev. D 103 (11) (2021) 116006, doi:10.1103/PhysRevD.103.116006, [2102.12541](#).
- [67] Gernot Eichmann, Christian S. Fischer, Unified description of hadron-photon and hadron-meson scattering in the Dyson-Schwinger approach, Phys. Rev. D 85 (2012) 034015, doi:10.1103/PhysRevD.85.034015, [1111.0197](#).
- [68] Pieter Maris, Peter C. Tandy, The Quark photon vertex and the pion charge radius, Phys. Rev. C 61 (2000) 045202, doi:10.1103/PhysRevC.61.045202, [nucl-th/9910033](#).
- [69] Jorge Segovia, Bruno El-Bennich, Eduardo Rojas, Ian C. Cloet, Craig D. Roberts, Shu-Sheng Xu, Hong-Shi Zong, Completing the picture of the Roper resonance, Phys. Rev. Lett. 115 (17) (2015) 171801, doi:10.1103/PhysRevLett.115.171801, [1504.04386](#).
- [70] Arlene C. Aguilar, et al., Pion and Kaon Structure at the Electron-Ion Collider, Eur. Phys. J. A 55 (10) (2019) 190, doi:10.1140/epja/i2019-12885-0, [1907.08218](#).
- [71] Stephen R. Cotanch, Pieter Maris, QCD based quark description of pi pi scattering up to the sigma and rho region, Phys. Rev. D 66 (2002) 116010, doi:10.1103/PhysRevD.66.116010, [hep-ph/0210151](#).
- [72] Gernot Eichmann, Christian S. Fischer, Nucleon Compton scattering in the Dyson-Schwinger approach, Phys. Rev. D 87 (3) (2013) 036006, doi:10.1103/PhysRevD.87.036006, [1212.1761](#).
- [73] Jan Horak, Joannis Papavassiliou, Jan M. Pawłowski, Nicolas Wink, Ghost spectral function from the spectral Dyson-Schwinger equation, Phys. Rev. D 104 (2021), doi:10.1103/PhysRevD.104.074017, [2103.16175](#).
- [74] Anton K. Cyrol, Mario Mitter, Jan M. Pawłowski, Nils Strodthoff, Nonperturbative quark, gluon, and meson correlators of unquenched QCD, Phys. Rev. D 97 (5) (2018) 054006, doi:10.1103/PhysRevD.97.054006, [1706.06326](#).
- [75] Alexandre F. Falcão, Orlando Oliveira, Paulo J. Silva, Analytic structure of the lattice Landau gauge gluon and ghost propagators, Phys. Rev. D 102 (11) (2020) 114518, doi:10.1103/PhysRevD.102.114518, [2008.02614](#).
- [76] Ayşe Kızılersü, Orlando Oliveira, Paulo J. Silva, Jon-Ivar Skullerud, André Sternbeck, Quark-gluon vertex from Nf=2 lattice QCD, Phys. Rev. D 103 (11) (2021) 114515, doi:10.1103/PhysRevD.103.114515, [2103.02945](#).
- [77] A. C. Aguilar, F. De Soto, M. N. Ferreira, J. Papavassiliou, F. Pinto-Gómez, J. Rodríguez-Quintero, L. R. Santos, Nonperturbative four-gluon vertex in soft kinematics, Phys. Lett. B 858 (2024) 139065, doi:10.1016/j.physletb.2024.139065, [2408.06135](#).
- [78] F. Pinto-Gómez, F. De Soto, J. Rodríguez-Quintero, Complete analysis of the Landau-gauge three-gluon vertex from lattice QCD, Phys. Rev. D 110 (1) (2024) 014005, doi:10.1103/PhysRevD.110.014005, [2404.08777](#).
- [79] Markus Q. Huber, Christian S. Fischer, Helios Sanchis-Alepuz, Higher spin glueballs from functional methods, Eur. Phys. J. C 81 (12) (2021) 1083, doi:10.1140/epjc/s10052-021-09864-5, [Erratum: Eur.Phys.J.C 82, 38 (2022)], [2110.09180](#).